JOURNAL OF GUIDANCE, CONTROL, AND DYNAMICS
Vol. 31, No. 5, September–October 2008

Adaptive Control of Advanced Fighter Aircraft in Nonlinear Flight Regimes

Yoonghyun Shin*
Agency for Defense Development, Daejeon 305-600, Republic of Korea
Anthony J. Calise†
Georgia Institute of Technology, Atlanta, Georgia 30332
and
Matthew D. Johnson‡
Science Applications International Corporation, Huntsville, Alabama 35802

DOI: 10.2514/1.30213

When advanced fighter aircraft fly at high angles of attack, unsteady aerodynamic effects, wing rock, and saturation of aerodynamic effectors can lead to difficulty in control and maneuverability. A novel adaptive output feedback control design based on dynamic inversion is investigated for aircraft which are operated in highly nonlinear flight regimes, where uncertainties in the form of both unmodeled parameter variations and unmodeled dynamics are common. The stability of the design is analyzed and validated with simulations using a modified NASA F-15 simulation. The simulation includes thrust vectoring and a differential stabiliator to provide increased control authority at high angles of attack and relaxed static stability to increase pitch maneuverability. The control designs include the use of "pseudocontrol hedging" techniques to exclude adaptation to control saturation.

Nomenclature

$\mathbf{E}$	=	output tracking error vector
$\tilde{\mathbf{E}}$	=	observer error vector
$\hat{\mathbf{E}}$	=	linear observer vector
$h_i(\cdot)$	=	ith Lie derivative of the system output function $h(\cdot)$
$\hat{h}_i(\cdot)$	=	approximation of $h_i(\cdot)$
K_P, K_D	=	proportional gain and derivative gain of the dynamic compensator
L, M, N	=	rolling, pitching, and yawing moments
n_1, n_2, n_3	=	numbers of neural network inputs, neurons, and outputs
p_s, r_s	=	stability axis roll and yaw rates
q	=	pitch rate
$\mathbf{r}$	=	vector relative degree
r_t	=	total degree (sum of elements in $\mathbf{r}$)
S_p, S_α, S_β	=	thrust vector scheduling variables in x, y, and z axes
$\mathbf{u}$	=	control input vector
W, V	=	inner- and outer-layer network weights
$\mathbf{x}$	=	state vector
$\mathbf{y}$	=	output vector
$\bar{\mathbf{y}}$	=	regulated output vector
$\mathbf{y}_c$	=	commanded output vector
$\mathbf{y}_M$	=	reference model state vector
α, β	=	angle of attack and sideslip angles
Γ_v, Γ_w, κ_v, κ_w	=	adaptation gains
$\boldsymbol{\Delta}(\cdot)$	=	modeling error function
δ_a, δ_e, δ_r	=	aileron, elevator, and rudder deflection angles
δ_{p1}, δ_{p2}, δ_{y1}, δ_{y2}	=	pitch and yaw vectoring angles of the left and right engines
$\boldsymbol{\mu}$	=	neural network input vector
$\boldsymbol{\nu}$	=	pseudocontrol
$\boldsymbol{\nu}_{\text{ad}}$	=	neural network output
$\boldsymbol{\nu}_{\text{dc}}$	=	dynamic compensator component of pseudocontrol
$\boldsymbol{\nu}_h$	=	pseudocontrol hedge
$\boldsymbol{\nu}_{\text{rm}}$	=	reference model component of pseudocontrol
$\boldsymbol{\xi}$	=	state vector associated with the output dynamics
$\boldsymbol{\sigma}(\cdot)$, $\boldsymbol{\sigma}'(\cdot)$	=	sigmoidal function and its gradient
ϕ, θ	=	roll and pitch angles
$\boldsymbol{\varphi}$	=	state vector associated with the internal dynamics
$\|\cdot\|$	=	Euclidean norm
$\|\cdot\|_F$	=	Frobenius norm

Presented as Paper 5717 at the AIAA Guidance, Navigation, and Control Conference and Exhibit, Austin, Texas, 11–14 August 2003; received 2 February 2007; revision received 11 February 2008; accepted for publication 11 February 2008.

*Senior Researcher, Yuseong Post Office Box 35; johnvshin@yahoo.com. Member AIAA.
†Professor, School of Aerospace Engineering, 270 Ferst Drive; anthony.calise@ae.gatech.edu. Fellow AIAA.
‡Avionics Engineer; matthew.d.johnson@saic.com. Member AIAA.

I. Introduction

NEWLY emerging aircraft are extending their flight envelopes over traditional flight regimes, leading to a need for substantially higher-performance control laws. Among these are the Joint Strike Fighter and F-22 which will be capable of operating at high angles of attack. At this flight condition both unmodeled parameter variations and unmodeled vehicle dynamics can occur, such as unsteady aerodynamic effects, saturation of aerodynamic effectors, and coupled longitudinal and lateral responses. These uncertainties present the main challenges in designing flight control systems for these regimes. Novel advanced control design methodologies are required to address the nonlinear and poorly understood aerodynamic characteristics of such vehicles.

Nonlinear dynamic inversion (NDI) [1,2] is a popular method of advanced flight control design. The chief advantage of NDI is that it avoids the gain-scheduling process of other methods, which is time consuming, costly, iterative, and labor intensive. NDI offers greater flexibility for handling changing models as an airframe evolves during its design cycle and greater ability to address nonstandard

flight regimes. Many designs of modern, advanced aerospace vehicles are now based on this technique [3–6]. A two-time scale, or two-stage dynamic inversion approach has been widely applied for highly maneuverable fighter aircraft [7–10] and unmanned aerial vehicles (UAVs) [9–11]. These studies have demonstrated that NDI is an effective method of control design for highly maneuverable aircraft. However, as noted in [7], NDI can be vulnerable to modeling and inversion errors. And so neural network based adaptive control design has been introduced to compensate for this deficiency [9–11].

Artificial neural networks (NNs) are any computing architecture that consists of massively parallel interconnections of simple computing elements. The superiority of NNs over other approximation methods is based on the fact that NNs are able to universally approximate smooth but otherwise arbitrary nonlinear functions on a compact set to any desired degree of accuracy using a sufficiently large number of NN elements [12–16].

In recent decades, there have been numerous research efforts to implement NNs as adaptive elements in nonlinear adaptive control designs [17–19]. In the 1990s, Narendra and Mukhopadhyay studied identification and control of linear and nonlinear systems using NNs [20]. Lewis et al. studied a state feedback linearly parameterized NN adaptive controller and multilayer NN structures with improved update laws [18–21]. Recently, Hovakimyan et al. developed single-hidden-layer (SHL) NN-based adaptive output feedback control of uncertain nonlinear systems assuming both the dynamics and the dimension of the regulated system may be poorly known, whereas the relative degree of the regulated output is assumed to be known [22]. In addition, they developed an adaptive output feedback control methodology for multi-input–multi-output (MIMO) nonlinear systems using linearly parameterized NNs [23].

Since the early 1990s, a great deal of research has been devoted to improving aircraft performance by designing NN-based adaptive flight control systems [24,25]. This research has included high performance fighters [4,10,26,27], tailless aircraft [5,9], missiles [28], tilt-rotor aircraft [29], UAVs [9,11,30], guided munitions [31], and helicopters [32,33]. Some of these papers have adopted the use of pseudocontrol hedging (PCH) [34]. PCH is a method for protecting an adaptive process from the effect of control nonlinearity due to position and rate limits.

This paper defines a design paradigm building on past results in the area of NN-based adaptive flight control which have been successfully used for a variety of aerospace applications [9,10,35,36], while incorporating recent advances in the areas of output feedback and adaptation under saturated control conditions. The method is based on approximate input–output feedback linearization and synthesis of a fixed-gain dynamic compensator, while incorporating SHL NNs to compensate for model inversion error.

The control design formulation and its stability analysis differ from previous work [23,37], in that the approach relies on a matching condition assumption that the uncertainties lie in the span of the control input matrix. We feel that this formulation is more straightforward from the perspective of dynamic inversion control and better suited to application in flight control. A consequence of this formulation is a new form for the observer error dynamics. A second contribution is a detailed application to flight control design of a vehicle capable of high-α supermaneuvers. To this end we employ a vehicle model that incorporates an existing baseline flight control system based on dynamic inversion. The aircraft model incorporates relaxed static stability (RSS) to permit high-α flight, differential stabiliator/tail (DT) control, thrust vector control (TVC), and control allocation.

The paper is organized as follows. Section II introduces input–output feedback linearization of nonlinear MIMO systems and NDI. Section III presents the structure and synthesis of linearly and nonlinearly parameterized NNs which are used in the remaining sections. Section IV illustrates adaptive NDI control design for MIMO output feedback systems, and the stability of the closed-loop system is proved using Lyapunov-like theorems. Section V presents an application of the NN-based adaptive control design to a highly maneuverable aircraft, the NASA F-15 ACTIVE (Advanced Control Technology for Integrated Vehicles) [38]. To manage control redundancy, a control allocation scheme is applied along with a thrust vector scheduling algorithm. Simulation results illustrate some of the benefits of the NN-based adaptive control design in Sec. VI. Section VII presents the main conclusions to be drawn from this effort.

II. Input–Output Feedback Linearization and Nonlinear Dynamic Inversion

Consider the nonlinear system

$$\dot{\mathbf{x}}(t) = \mathbf{f}(\mathbf{x}, \mathbf{u}) \qquad \mathbf{y}(t) = \mathbf{g}(\mathbf{x}) \tag{1}$$

where $\mathbf{x} \in \mathcal{D}_x \subset \Re^n$ is the state vector, $\mathbf{u} \in \mathcal{D}_u \subset \Re^m$ is the system control vector, and $\mathbf{y} \in \mathcal{D}_y \subset \Re^m$ is the system output vector.

Assumption 1. The system in Eq. (1) satisfies the conditions for output feedback linearization with well-defined vector relative degree $\mathbf{r}$.

By selecting the appropriate controlled variables for input–output feedback linearization, with this assumption it is possible to rewrite Eq. (1) in the following normal form:

$$\begin{aligned}
\dot{\boldsymbol{\varphi}} &= \mathbf{f}_o(\boldsymbol{\varphi}, \boldsymbol{\xi}) \\
\dot{\xi}_i^1 &= \xi_{i+1}^2 \\
&\vdots \\
\dot{\xi}_i^{r_i-1} &= \xi_i^{r_i} \\
\dot{\xi}_i^{r_i} &= h_i(\boldsymbol{\xi}, \boldsymbol{\varphi}, u_i) \\
y_i &= \xi_i^1, \qquad i = 1, \ldots, m
\end{aligned} \tag{2}$$

where

$$\boldsymbol{\xi} \triangleq \begin{bmatrix} \xi_1^1 & \xi_1^2 & \cdots & \xi_1^{r_1} & \cdots & \xi_m^1 & \xi_m^2 & \cdots & \xi_m^{r_m} \end{bmatrix}^T \in \Re^{r_t}$$

$$h_i(\boldsymbol{\xi}, \boldsymbol{\varphi}, u_i) \triangleq L_{\mathbf{f}}^{(r_i)} \mathbf{g}|_{u_i}$$

with $i = 1, \ldots, m$ being the Lie derivatives, and $\boldsymbol{\varphi} \in \mathcal{D}_\varphi \subset \Re^{n-r_t}$ is the state vector associated with the internal dynamics

$$\dot{\boldsymbol{\varphi}} = \mathbf{f}_o(\boldsymbol{\varphi}, \boldsymbol{\xi}) \tag{3}$$

where

$$r_t \triangleq r_1 + r_2 + \cdots + r_m \leq n$$

The functions $\mathbf{f}_o(\boldsymbol{\xi}, \boldsymbol{\varphi})$ and $h_i(\boldsymbol{\xi}, \boldsymbol{\varphi}, u_i)$ are assumed to be partially known and continuous functions of their arguments.

Assumption 2. The internal dynamics in Eq. (3) are input-to-state stable [39].

Assumption 3. $\partial h_i(\mathbf{x}, u_i)/\partial u_i$ is continuous and nonzero for every $(\mathbf{x}, u_i) \in \mathcal{D}_x \times \Re$.

A linearizing feedback control law is approximated by introducing the following signal:

$$u_i = \hat{h}_i^{-1}(\mathbf{y}, \nu_i), \qquad i = 1, \ldots, m \tag{4}$$

where ν_i, commonly referred to as the pseudocontrol, is defined as

$$\nu_i = \hat{\mathbf{h}}_i(\mathbf{y}, u_i), \qquad i = 1, \ldots, m \tag{5}$$

Assumption 4. $\partial \hat{h}_i(\mathbf{y}, u_i)/\partial u_i$ is continuous and nonzero for every $(\mathbf{y}, u_i) \in \mathcal{D}_y \times \Re$, and

$$\frac{\partial \hat{h}_i(\mathbf{y}, u_i)}{\partial u_i} \frac{\partial h_i(\mathbf{x}, u_i)}{\partial u_i} > 0, \qquad i = 1, \ldots, m \tag{6}$$

for every $(\mathbf{x}, \mathbf{y}, u_i) \in \mathcal{D}_x \times \mathcal{D}_y \times \Re$.

Defining $\boldsymbol{\nu} = [\, \nu_1 \quad \cdots \quad \nu_m \,]^T$, we rewrite Eq. (5) in a compact form as

$$\boldsymbol{\nu} = \hat{\mathbf{h}}(\mathbf{y}, \mathbf{u}) \tag{7}$$

With this definition of pseudocontrol, the output dynamics can be expressed as

$$\mathbf{y}^{(r)} = \boldsymbol{\nu} + \Delta_x(\mathbf{x}, \mathbf{u}) \tag{8}$$

where $\mathbf{y}^{(r)} = [\, y_1^{(r_1)} \quad \cdots \quad y_m^{(r_m)} \,]^T$ and

$$\boldsymbol{\Delta}_x(\mathbf{x}, \mathbf{u}) = \boldsymbol{\Delta}(\boldsymbol{\xi}, \boldsymbol{\varphi}, \mathbf{u}) = \mathbf{h}(\boldsymbol{\xi}, \boldsymbol{\varphi}, \hat{\mathbf{h}}^{-1}(\mathbf{y}, \boldsymbol{\nu})) - \hat{\mathbf{h}}(\mathbf{y}, \hat{\mathbf{h}}^{-1}(\mathbf{y}, \boldsymbol{\nu})) \tag{9}$$

which is referred to as the modeling error.

III. Neural Network and Its Parameterization

A smooth nonlinear function $\boldsymbol{\Delta}_x(\mathbf{x})$: $\Re^n \to \Re^m$ can be nonlinearly parameterized by an SHL NN over a sufficiently large compact region of interest $(\mathbf{x}, \mathbf{u}) \in \mathcal{D} \subset \mathcal{D}_x \times \Re^m$ in the state space to within arbitrary accuracy, given a sufficient number of hidden layer neurons and sufficient input information [17]. The input–output map of SHL NN in the multiple output case can be expressed as

$$\boldsymbol{\nu}_{\text{ad}} = \hat{W}^T \bar{\boldsymbol{\sigma}}(\hat{V}^T \boldsymbol{\mu}) \tag{10}$$

where the two NN weight matrices $\hat{V}$, $\hat{W}$ are estimates of the ideal inner- and outer-layer weight matrices $V \in \Re^{(n_1+1)\times n_2}$ and $W \in \Re^{(n_2+1)\times n_3}$. The vector function $\bar{\boldsymbol{\sigma}}(\hat{V}^T \boldsymbol{\mu})$ is defined by

$$\bar{\boldsymbol{\sigma}}(z) = [\, 1 \quad \sigma(z_1) \quad \sigma(z_2) \quad \cdots \quad \sigma(z_{n_2}) \,]^T \in \Re^{n_2+1} \tag{11}$$

The scalar function $\sigma(\cdot)$ is a sigmoidal activation function that is typically of the form

$$\sigma(z) = 1/(1 + e^{-az}) \tag{12}$$

where the factor a is known as the activation potential and can be a distinct value for each neuron.

The weight matrices V, W are updated according to the following adaptation law [18,21]:

$$\begin{aligned} \dot{\hat{V}} &= -\Gamma_v \cdot [\boldsymbol{\mu} \mathbf{E}^T P B \hat{W}^T \hat{\boldsymbol{\sigma}}' + \kappa_v \cdot (\hat{V} - V_0)] \\ \dot{\hat{W}} &= -\Gamma_w \cdot [(\hat{\boldsymbol{\sigma}} - \hat{\boldsymbol{\sigma}}' \hat{V}^T \boldsymbol{\mu}) \mathbf{E}^T P B + \kappa_w \cdot (\hat{W} - W_0)] \end{aligned} \tag{13}$$

where $\hat{\boldsymbol{\sigma}} = \boldsymbol{\sigma}(\hat{V}^T \boldsymbol{\mu})$ and $\boldsymbol{\sigma}' = \text{diag}(\text{d}\sigma_i/\text{d}z_i)$ denotes the Jacobian matrix. W_0 and V_0 are initial guesses, Γ_v, Γ_w, κ_v, and $\kappa_w > 0$ are adaptation gains, and P is a solution of the Lyapunov equation

$$A^T P + P A = -Q, \qquad Q > 0 \tag{14}$$

For this case, the NN approximation error can be expressed in the form [21,22]:

$$\begin{aligned} \boldsymbol{\Delta}_x(\mathbf{x}) - \boldsymbol{\nu}_{\text{ad}} &= W^T \bar{\boldsymbol{\sigma}}(V^T \boldsymbol{\mu}) - \hat{W}^T \bar{\boldsymbol{\sigma}}(\hat{V}^T \boldsymbol{\mu}) + \boldsymbol{\varepsilon}(\mathbf{x}) \\ &= \tilde{W}^T (\hat{\boldsymbol{\sigma}} - \hat{\boldsymbol{\sigma}}' \hat{V}^T \boldsymbol{\mu}) + \hat{W}^T \hat{\boldsymbol{\sigma}}' \tilde{V}^T \boldsymbol{\mu} + \boldsymbol{\varepsilon}(\mathbf{x}) - \mathbf{w} \end{aligned} \tag{15}$$

where $\tilde{W} \triangleq W - \hat{W}$, $\tilde{V} \triangleq V - \hat{V}$ are NN estimation errors, and the error $\boldsymbol{\varepsilon}(\mathbf{x}) - \mathbf{w}$ is bounded such that

$$\|\boldsymbol{\varepsilon}(\mathbf{x}) - \mathbf{w}\| \le \gamma_1 \|\tilde{Z}\|_F + \gamma_2 \tag{16}$$

γ_1, γ_2 are positive computable constants, and

$$\tilde{Z} \triangleq \begin{bmatrix} \tilde{W} & 0 \\ 0 & \tilde{V} \end{bmatrix} \tag{17}$$

Further,

$$\begin{aligned} \|\boldsymbol{\Delta}_x - \boldsymbol{\nu}_{\text{ad}}\| &= \|W^T \boldsymbol{\sigma}(V^T \boldsymbol{\mu}) - \hat{W}^T \boldsymbol{\sigma}(\hat{V}^T \boldsymbol{\mu}) + \boldsymbol{\varepsilon}(\mathbf{x}) - \mathbf{w}\| \\ &\le \alpha_1 \|\tilde{Z}\|_F + \alpha_2 \end{aligned} \tag{18}$$

where $\alpha_1 = \sqrt{n_2 + 1}$, and $\alpha_2 = 2\sqrt{n_2 + 1} W^* + \varepsilon_m$ with $\|W\|_F < W^*$.

In Eq. (10), $\boldsymbol{\mu}$ is normally taken as $\mathbf{x}$ in the state feedback case. In the output feedback case only $\mathbf{y}$ is available. However, when the system is observable from difference quotients of its input–output history, a universal approximation property of SHL NN for the output feedback case can be defined using the measurement and control variables, having time delay d [23,40].

IV. Adaptive NDI Control Design

A reference model, adaptive NDI control architecture, and linear observer are introduced in this section. Stability analysis with SHL NNs using Lyapunov theorems is performed to show that all the error signals and internal signals in the resultant closed-loop system are bounded.

A. Reference Model

Introducing a bounded external disturbance $\mathbf{d}(t) \in \Re^m$, Eq. (8) can be written in the form that assumes that both the uncertainties and disturbances are matched,

$$\dot{\bar{\mathbf{y}}}(t) = A \bar{\mathbf{y}}(t) + B[\boldsymbol{\nu}(t) + \Delta_x(\mathbf{x}, \mathbf{u}) + \mathbf{d}(t)] \tag{19}$$

where

$$\begin{aligned} \bar{\mathbf{y}} &\triangleq [\, \mathbf{y}_1^T \quad \mathbf{y}_2^T \quad \cdots \quad \mathbf{y}_m^T \,]^T \in \Re^{r_t} \\ \mathbf{y}_i &\triangleq [\, y_i \quad \dot{y}_i \quad \cdots \quad y_i^{(r_i-1)} \,]^T \in \Re^{r_i}, \qquad i = 1, \ldots, m \\ A &\triangleq \text{block-diag}(\, A_1 \quad A_2 \quad \cdots \quad A_m \,) \in \Re^{r_t \times r_t} \\ B &\triangleq \text{block-diag}(\, B_1 \quad B_2 \quad \cdots \quad B_m \,) \in \Re^{r_t \times m} \end{aligned} \tag{20}$$

and

$$A_i = \begin{bmatrix} 0 & 1 & 0 & \cdots & 0 & 0 \\ 0 & 0 & 1 & \cdots & 0 & 0 \\ \vdots & \vdots & \vdots & \ddots & \vdots & \vdots \\ 0 & 0 & 0 & \cdots & 0 & 1 \\ 0 & 0 & 0 & \cdots & 0 & 0 \end{bmatrix} \in \Re^{r_i \times r_i}, \qquad B_i = \begin{bmatrix} 0 \\ 0 \\ \vdots \\ 0 \\ 1 \end{bmatrix} \in \Re^{r_i \times 1} \tag{21}$$

$$\|\mathbf{d}(t)\| \le d_m \tag{22}$$

A reference model is described by an equation which is composed of m sets of ordinary differential equations having r_i^{th}, $i = 1, \ldots, m$ order, respectively. The system of reference model equations can be written in a compact state-space form as

$$\dot{\mathbf{y}}_M(t) = A_M \mathbf{y}_M(t) + B_M \cdot \mathbf{y}_c(t) \tag{23}$$

where

$$\begin{aligned} \mathbf{y}_M &\triangleq \begin{bmatrix} \mathbf{y}_{M_1}^T & \mathbf{y}_{M_2}^T & \cdots & \mathbf{y}_{M_m}^T \end{bmatrix}^T \in \Re^{r_t} \\ \mathbf{y}_{M_i} &\triangleq \begin{bmatrix} y_{M_i} & \dot{y}_{M_i} & \cdots & y_{M_i}^{(r_i-1)} \end{bmatrix}^T \in \Re^{r_i}, \qquad i = 1, \ldots, m \\ \mathbf{y}_c &\triangleq \begin{bmatrix} y_{c_1} & y_{c_2} & \cdots & y_{c_m} \end{bmatrix}^T \in \Re^m \\ A_M &\triangleq \text{block-diag}(\, A_{M_1} \quad A_{M_2} \quad \cdots \quad A_{M_m} \,) \in \Re^{r_t \times r_t} \\ B_M &\triangleq \text{block-diag}(\, B_{M_1} \quad B_{M_2} \quad \cdots \quad B_{M_m} \,) \in \Re^{r_t \times m} \end{aligned} \tag{24}$$

and

$$A_{M_i} = \begin{bmatrix} 0 & 1 & 0 & \cdots & 0 & 0 \\ 0 & 0 & 1 & \cdots & 0 & 0 \\ \vdots & \vdots & \vdots & \ddots & \vdots & \vdots \\ 0 & 0 & 0 & \cdots & 0 & 1 \\ -a_{i1} & -a_{i2} & -a_{i3} & \cdots & -a_{i(r_i-1)} & -a_{ir_i} \end{bmatrix} \in \Re^{r_i \times r_i}$$

$$B_{M_i} = \begin{bmatrix} 0 \\ 0 \\ \vdots \\ 0 \\ a_{i1} \end{bmatrix} \in \Re^{r_i \times 1} \tag{25}$$

$\mathbf{y}_c(t) \in \Re^m$ is a bounded piecewise continuous reference command, and A_M is Hurwitz.

In model reference adaptive control, the objective is to design a control law such that the output tracking error

$$\mathbf{E}(t) = \mathbf{y}_M(t) - \bar{\mathbf{y}}(t) \tag{26}$$

tends to zero and all the signals in the system remain bounded. In NN-based adaptive control, because of the network reconstruction error, the goal is to show that $\mathbf{E}(t)$ is uniformly ultimately bounded. Furthermore, because the universal approximation property holds only on a compact set, the result at best can only be semiglobal.

B. Adaptive NDI Control Architecture

The pseudocontrol is chosen to have the form

$$\boldsymbol{\nu}(t) \triangleq \underbrace{K_e \cdot \hat{\mathbf{E}}(t)}_{\boldsymbol{\nu}_{\mathrm{dc}}} + \underbrace{K_r \cdot \mathbf{y}_c(t) - K_e \cdot \mathbf{y}_M(t)}_{\boldsymbol{\nu}_{rm}} - \boldsymbol{\nu}_{\mathrm{ad}} \tag{27}$$

where $\hat{\mathbf{E}}(t)$ is the state of a linear observer of the tracking error $\mathbf{E}(t)$, and the feedback gain $K_e \in \Re^{m \times r_t}$ and the feedforward gain $K_r \in \Re^{m \times m}$ are such that

$$\|K_e\| < k_{em}, \qquad \|K_r\| < k_{rm} \tag{28}$$

Figure 1 illustrates the overall architecture of the adaptive control design. The linear observer is defined in the next section. Substituting Eq. (27) into the system dynamics Eq. (19) results in the closed-loop system

$$\dot{\bar{\mathbf{y}}}(t) = (A - BK_e)\bar{\mathbf{y}}(t) + BK_r\mathbf{y}_c(t) + B(\boldsymbol{\Delta}_x - \boldsymbol{\nu}_{\mathrm{ad}} + \mathbf{d} - K_e\tilde{\mathbf{E}}) \tag{29}$$

where $\tilde{\mathbf{E}} \triangleq \mathbf{E} - \hat{\mathbf{E}}$.

This formulation differs from earlier formulations [23,37] in that a dynamic compensator is not employed in formulating the pseudocontrol in Eq. (27). This significantly simplifies the controller structure and reduces the dimension of the error observer to be described in the next section. The simplification comes about due to the fact that $\tilde{\mathbf{E}}$ is matched in Eq. (29). Therefore if $\boldsymbol{\nu}_{\mathrm{ad}}$ cancels $\boldsymbol{\Delta}_x(\mathbf{x}, \mathbf{u}) + \mathbf{d}$, and if $\tilde{\mathbf{E}}$ asymptotically goes to zero, then by choosing K_e such that $(A - BK_e)$ is Hurwitz, $\bar{\mathbf{y}}(t)$ asymptotically goes to zero. More realistically, if $\boldsymbol{\Delta}_x - \boldsymbol{\nu}_{\mathrm{ad}} + \mathbf{d} - K_e\tilde{\mathbf{E}}$ is bounded and the initial condition $\bar{\mathbf{y}}(0)$ lies within the approximation domain of the NN, then $\bar{\mathbf{y}}(t)$ is uniformly ultimately bounded, and because of Assumption 2, so is $\boldsymbol{\varphi}(t)$.

A particularly simple form for the error dynamics results if we choose K_e and K_r such that

$$A - BK_e = A_M, \qquad BK_r = B_M \tag{30}$$

Examining the forms of A, A_m, B, and B_m in Eqs. (19) and (23), it is easy to see that this can always be done. With this choice, the closed-loop dynamics of the tracking error signal $\mathbf{E}(t)$ in Eq. (26) can be expressed in the form

$$\dot{\mathbf{E}}(t) = A_M\mathbf{E}(t) - B(\boldsymbol{\Delta}_x - \boldsymbol{\nu}_{\mathrm{ad}} + \mathbf{d} - K_e\tilde{\mathbf{E}}), \qquad z = C\mathbf{E}(t) \tag{31}$$

where $z \in \Re^m$ is the vector of available measurements, $C = \text{block-diag}(\mathbf{c}_i) \in \Re^{m \times r_t}$, $i = 1, \ldots, m$, and $\mathbf{c}_i = [1 \quad 0 \quad \cdots \quad 0] \in \Re^{1 \times r_i}$. Because A_M is Hurwitz, there exists a unique and positive definite matrix $P = P^T > 0$ satisfying

$$A_M^T P + PA_M = -Q \tag{32}$$

for any $Q = Q^T > 0$

It can be seen from Eq. (9) that $\boldsymbol{\Delta}_x$ depends on $\boldsymbol{\nu}_{\mathrm{ad}}$ through $\boldsymbol{\nu}$. Because $\boldsymbol{\nu}_{\mathrm{ad}}$ is the output of a NN, the term $\boldsymbol{\nu}_{\mathrm{ad}} - \boldsymbol{\Delta}_x(\mathbf{x}, \mathbf{u})$ will be referred to as the NN approximation error.

C. Linear Observer of Error Dynamics

We consider the case of a full-order observer of dimension r_t for the tracking error dynamics in Eq. (31)

$$\dot{\hat{\mathbf{E}}}(t) = A_M\hat{\mathbf{E}}(t) + F(\mathbf{z} - \hat{\mathbf{z}}), \qquad \hat{\mathbf{z}} = C\hat{\mathbf{E}} \tag{33}$$

where F is a gain matrix, and should be chosen such that $A_M - FC$ is asymptotically stable, and $\mathbf{z}$ is defined in Eq. (31). Let

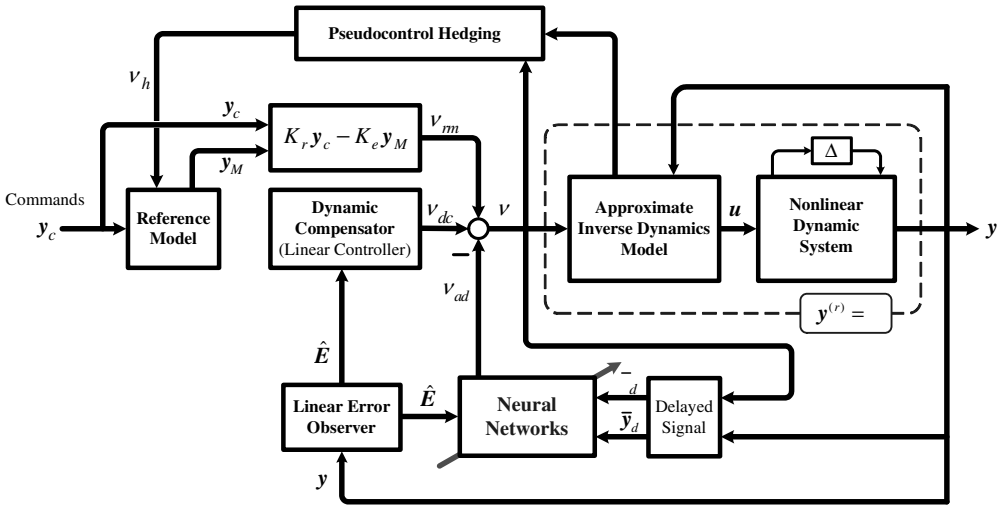

Fig. 1 Adaptive nonlinear dynamic inversion control design architecture.

$$\tilde{A} \triangleq A_M - FC \tag{34}$$

Then the observer error dynamics can be written as

$$\dot{\tilde{\mathbf{E}}}(t) = \tilde{A}\,\tilde{\mathbf{E}}(t) - B(\boldsymbol{\Delta}_x - \boldsymbol{\nu}_{\text{ad}} + \mathbf{d} - K_e\tilde{\mathbf{E}}) \tag{35}$$

Since $\tilde{A}$ is Hurwitz, there exists a unique and positive definite matrix $\tilde{P} = \tilde{P}^T > 0$ for an arbitrary matrix $\tilde{Q} = \tilde{Q}^T > 0$ satisfying the Lyapunov equation

$$\tilde{A}^T\tilde{P} + \tilde{P}\tilde{A} = -\tilde{Q} \tag{36}$$

D. Stability Analysis

Using Lyapunov's direct method we show that the closed-loop system is uniformly ultimately bounded. To this end we consider an error vector

$$\boldsymbol{\zeta} = [\,\mathbf{E}^T \quad \tilde{\mathbf{E}}^T \quad \text{vec}\tilde{W}^T \quad \text{vec}\tilde{V}^T\,]^T \tag{37}$$

and a positive definite Lyapunov function candidate

$$\mathcal{L}(\boldsymbol{\zeta}) = \mathbf{E}^T P\mathbf{E} + \tilde{\mathbf{E}}^T\tilde{P}\,\tilde{\mathbf{E}} + \text{tr}\left(\tilde{W}^T\Gamma_w^{-1}\tilde{W} + \tilde{V}^T\Gamma_v^{-1}\tilde{V}\right) \tag{38}$$

In the expanded space of the compound error variable, consider the largest level set of $\mathcal{L}(\boldsymbol{\zeta})$ in $\mathcal{D}_\zeta$ such that its projection on the subspace of the NN input variables completely lies in $\mathcal{D}$. As shown in Fig. 2, define the largest ball that lies inside that level set as

$$B_R \triangleq \{\boldsymbol{\zeta} \mid \|\boldsymbol{\zeta}\| \le R\} \tag{39}$$

and let α be the minimum value of $\mathcal{L}(\boldsymbol{\zeta})$ on the boundary of B_R

$$\alpha \triangleq \min_{\|\boldsymbol{\zeta}\|=R} \mathcal{L}(\boldsymbol{\zeta}) \tag{40}$$

Introduce the set

$$\Omega_\alpha \triangleq \{\boldsymbol{\zeta} \in B_R | \mathcal{L}(\boldsymbol{\zeta}) \le \alpha\} \tag{41}$$

From the definition of the candidate Lyapunov function $\mathcal{L}$ in Eq. (38), there exist class $\mathcal{K}$ functions χ_1 and χ_2 such that

$$\chi_1(\boldsymbol{\zeta}) \le \mathcal{L}(\|\boldsymbol{\zeta}\|) \le \chi_2(\boldsymbol{\zeta}) \tag{42}$$

where

$$\begin{aligned}\chi_1(\|\boldsymbol{\zeta}\|) &= \lambda_{\min}(P)\|\mathbf{E}\|^2 + \lambda_{\min}(\tilde{P})\|\tilde{\mathbf{E}}\|^2 + \lambda_{\min}\left(\Gamma_w^{-1}\right)\|\tilde{W}\|_F^2 \\ &\quad + \lambda_{\min}\left(\Gamma_v^{-1}\right)\|\tilde{V}\|_F^2 \\ \chi_2(\|\boldsymbol{\zeta}\|) &= \lambda_{\max}(P)\|\mathbf{E}\|^2 + \lambda_{\max}(\tilde{P})\|\tilde{\mathbf{E}}\|^2 + \lambda_{\max}\left(\Gamma_w^{-1}\right)\|\tilde{W}\|_F^2 \\ &\quad + \lambda_{\max}\left(\Gamma_v^{-1}\right)\|\tilde{V}\|_F^2\end{aligned} \tag{43}$$

Assumption 5.

$$R > \chi_1^{-1}(\chi_2(\lambda)) \tag{44}$$

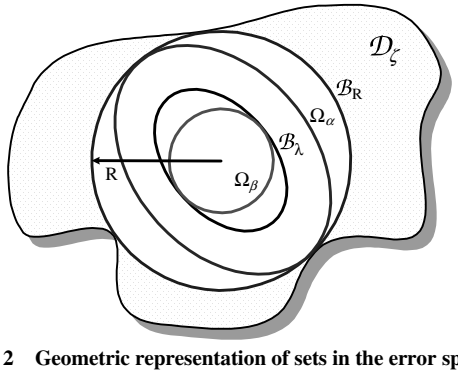

Fig. 2 Geometric representation of sets in the error space.

where λ is defined as

$$\lambda \triangleq \frac{\sqrt{2\alpha_1 p_a + 2\gamma_1(\gamma_2 + d_m)\|PB\| + \kappa_w\|W - W_0\|_F^2 + \kappa_v\|V - V_0\|_F^2}}{\min(\Lambda_1, \Lambda_2, \Lambda_3)} \tag{45}$$

and

$$\begin{aligned}\Lambda_1 &= \sqrt{\lambda_{\min}(Q) - \gamma_1\|PB\|(1 + \gamma_2 + d_m) - 2p_a k_{em}} \\ \Lambda_2 &= \sqrt{\lambda_{\min}(\tilde{Q}) - 2p_a(\alpha_1 + \alpha_2) - \gamma_1\|PB\|(1 + \gamma_2 + d_m) - 6p_a k_{em}} \\ \Lambda_3 &= \sqrt{\kappa_a - 2\alpha_1 p_a - 2\gamma_1\|PB\|}\end{aligned} \tag{46}$$

Theorem 1. Let Assumptions 1–5 hold. Then, if $\boldsymbol{\zeta}(0) \in \Omega_\alpha$, the control law given by Eq. (27), along with the NN adaptation law in Eq. (13), guarantees that the signals $\mathbf{E}$, $\tilde{\mathbf{E}}$, $\tilde{V}$, and $\tilde{W}$ and all the remaining signals in the closed-loop system, Eqs. (1), (13), (23), and (27), are uniformly ultimately bounded.

Proof. See the Appendix. □

Note: Assumptions 1–4 are standard [22,23,37] and are needed for smooth development of the control design based on approximate output feedback linearization. Assumption 1 is needed to express the system in normal form. Assumption 2 is required to ensure internal stability of the closed-loop system. In effect it assumes that the plant being inverted is minimum phase. Assumption 3 is needed to ensure that control effectiveness does not vanish, and Assumption 4 amounts to assuming that the sign of the control effectiveness is known for each actuator, a standard assumption in nearly all of the adaptive control literature. Assumption 5 assures the inclusion relationship between B_λ and B_R in Eq. (A9).

V. NN-Based Adaptive NDI Control Design for F-15 ACTIVE

This section applies the NN-based adaptive feedback control design to a modified F-15 simulation model with thrust-vectoring capability and RSS. The effects of control saturation are directly accounted for in the design of the adaptive controller using the PCH method [34].

A. Control Effectors

Maneuvering an aircraft in highly nonlinear flight regimes or at high α requires sufficient control authority. To enhance the maneuverability of the vehicle, we incorporate models for the differential stabilator, TVC, as well as introducing RSS.

TVC nozzles are modeled using the pitch/yaw balance beam nozzles (P/YBBN) of the F-15 ACTIVE aircraft [36], which allow at most 20 deg of nozzle deflection in any direction. Vectoring the thrust lines can generate pitching, yawing, and rolling moments by deflecting the nozzles synchronously or differentially as required. Because full deflection of TVC in one direction is only achievable when the other direction has zero deflection, an axis priority strategy is required. As depicted in Fig. 3, priority is given to the pitch/roll angle direction, that is, the nozzle first follows the pitch/roll command to the extent possible and then follows the yaw command with whatever control authority remains. To maximize the rolling moment achievable by aerodynamic controls, differential deflection of two horizontal stabilators, defined by $\delta_{DT} = (\delta_{e_{\text{right}}} - \delta_{e_{\text{left}}})/2$, is also employed [38].

B. High-α Aerodynamics

High-α aerodynamics are inherently associated with separated flows, vortices, and thus nonlinear aerodynamics. It is well known that an aerodynamic model for this regime requires a large amount of data mainly coming from wind-tunnel testing [41]. Unsteady aerodynamics are a representative phenomenon in the longitudinal

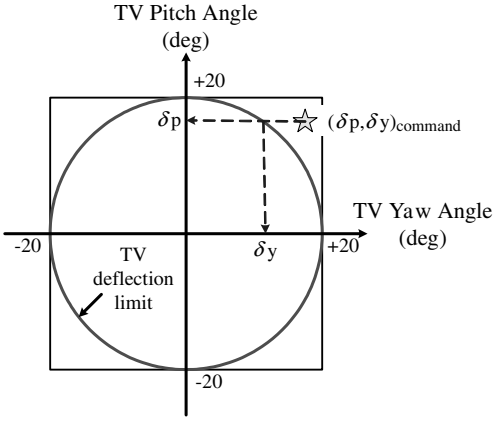

Fig. 3 Thrust-vectoring angle limit and priority.

axis in that they severely affect the pitch moment during high-α maneuvers. Asymmetric vortex flows and bursts at high α cause unpredictable rolling and yawing moments in lateral/directional axes, which result in unstable aerodynamic moment coefficients in this regime. Convention aerodynamic control surfaces become ineffective at high α, therefore TVC is introduced to maintain controllability [42–44].

One of the main objectives of the adaptive control design is to demonstrate adaptation to aerodynamic uncertainty in the form of both unmodeled parameter variations and unmodeled dynamics not accounted for in the nominal inverting control design. To this end, unsteady hypothetical aerodynamic terms and nonlinear damping are introduced.

1. Unsteady Aerodynamics

High-α flight with large amplitude maneuvers is affected by unsteady aerodynamic effects such as aerodynamic lag on the wings especially in the poststall region. A modified version of an unsteady aerodynamic model based on indicial functions was adopted [45]. The model in longitudinal axis can be expressed as

$$\begin{bmatrix} \dot{\alpha} \\ \dot{q} \\ \dot{x}_\alpha \end{bmatrix} = \begin{bmatrix} Z_\alpha & Z_q & 0 \\ C & M_q & B \\ 1 & 0 & -b_1 \end{bmatrix} \begin{bmatrix} \alpha \\ q \\ x_\alpha \end{bmatrix} + \begin{bmatrix} Z_\delta \\ M_\delta \\ 0 \end{bmatrix} \cdot \delta \tag{47}$$

where

$$B = \frac{\rho V^2 S\bar{c}}{2I_{yy}} a b_1, \qquad C = \frac{\rho V^2 S\bar{c}}{2I_{yy}} c \tag{48}$$

$a = 0.25$, $c = -0.23$, and $b_1 = 1.0$.

2. Lateral/Directional Aerodynamics at High α

The three significant lateral/directional aerodynamic damping coefficients used in the aircraft model are presented in Fig. 4, where positive values for C_{l_p} and C_{n_r} at high α imply instability.

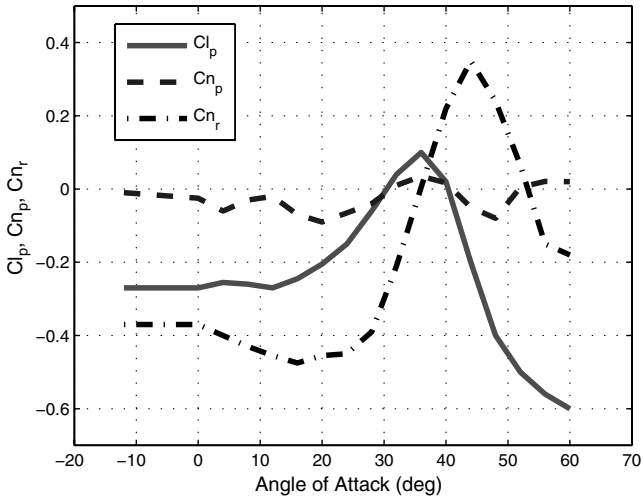

Fig. 4 Three dominant lateral/directional aerodynamic damping coefficients.

C. Implementation of Adaptive Control Design

As shown in Fig. 1, the raw pilot commands are input to command filters to generate reference signals. PCH is used to protect the adaptive process from control saturation nonlinearities. Next, proportional and derivative (PD) controllers are used to follow the reference commands. The control commands are obtained by a two-stage dynamic inversion. The structure of the inverting law and its implementation is displayed in Fig. 5. To illustrate a design we assume that p_s, α, and β are commanded through a pilot's control stick and pedal inputs δ_{LAT}, δ_{LON}, and δ_{DIR}, respectively. The α and β feedbacks are assumed to be computed from inertial measurements.

1. Two-Stage Nonlinear Dynamic Inversion

A two-stage approach assumes that the state dynamics can be decomposed as follows [7,10]:

1) Stage 1 dynamics, $\mathbf{x}_1 = [\alpha \quad \dot{\alpha} \quad \beta \quad \dot{\beta} \quad \phi \quad \theta \quad V]^T$.

2) Stage 2 dynamics, $\mathbf{x}_2 = [p_s \quad q \quad r_s]^T$.

In both stages of the inversion, the equations of motion are expressed in the form

$$\dot{\mathbf{x}} = a(\mathbf{x}) + b(\mathbf{x})\mathbf{u}, \qquad \mathbf{y} = C\mathbf{x} \tag{49}$$

where $\mathbf{y}$ defines the regulated variables and $\mathbf{u}$ defines the control variables, which are the output variables of the inverting blocks in the figure.

The control variables for the stage 1 dynamics are the angular accelerations in the roll, pitch, and yaw stability axis frame

$$\mathbf{u}_1 = [\dot{p}_{sc} \quad \dot{q}_{sc} \quad \dot{r}_{sc}]^T \tag{50}$$

and the control variables for the stage 2 dynamics are the effective control displacement commands in each axis

$$\mathbf{u}_2 = [\delta_{ac} \quad \delta_{ec} \quad \delta_{rc}]^T \tag{51}$$

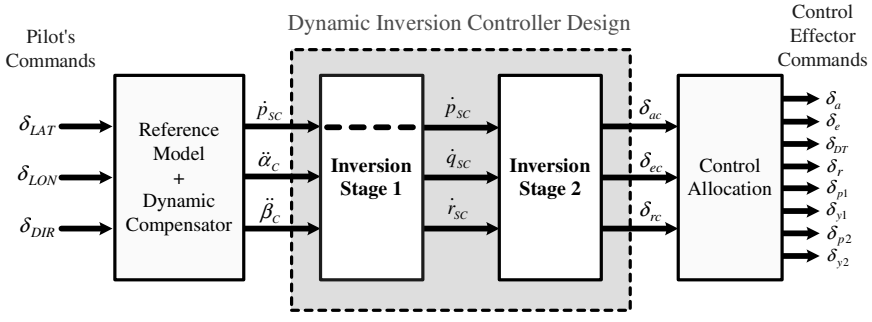

Fig. 5 Two-stage dynamic inversion control law structure.

Assuming $Cb(\mathbf{x})$ is invertible, then the inverting design in each stage is based on

$$\dot{\mathbf{y}} = Ca(\mathbf{x}) + Cb(\mathbf{x})\mathbf{u} = \boldsymbol{\nu} \tag{52}$$

where $\boldsymbol{\nu}$ is the pseudocontrol. The pseudocontrol is a linear control law designed to regulate $\mathbf{y}$, and corresponds to the inputs to each inverting block in Fig. 5.

The regulated variables in each stage are

$$\mathbf{y}_1 = [\, p_s \quad \dot{\alpha} \quad \dot{\beta}\,]^T \qquad \mathbf{y}_2 = [\, p_s \quad q \quad r_s\,]^T \tag{53}$$

The variable p_s has a relative degree of 1, while α and β each have a relative degree of 2 (it is necessary to differentiate these variables twice before a control term appears). Therefore $\mathbf{y}_1$ is defined so that the control appears in the first derivative of each of it elements. The same is true for stage 2.

Full-Scale Stage 1 Dynamics

The stage 1 dynamics can be written in the following form:

$$\begin{bmatrix} \dot{\alpha} \\ \ddot{\alpha} \\ \dot{\beta} \\ \ddot{\beta} \\ \dot{\phi} \\ \dot{\theta} \\ \dot{V} \\ \ddot{V} \end{bmatrix} = \begin{bmatrix} f_1(\mathbf{x}) \\ f_2(\mathbf{x},\boldsymbol{\delta}) \\ f_3(\mathbf{x}) \\ f_4(\mathbf{x},\boldsymbol{\delta}) \\ f_5(\mathbf{x},\boldsymbol{\delta}) \\ f_6(\mathbf{x},\boldsymbol{\delta}) \\ f_7(\mathbf{x},\boldsymbol{\delta}) \\ f_8(\mathbf{x},\boldsymbol{\delta},\dot{\boldsymbol{\delta}}) \end{bmatrix} + \begin{bmatrix} 0 & 0 & 0 \\ -\tan(\beta) & 1 & 0 \\ 0 & 0 & 0 \\ 0 & 0 & -1 \\ 0 & 0 & 0 \\ 0 & 0 & 0 \\ 0 & 0 & 0 \\ 0 & 0 & 0 \end{bmatrix} \begin{bmatrix} \dot{p}_s \\ \dot{q} \\ \dot{r}_s \end{bmatrix} \tag{54}$$

where p_s and r_s denote the stability axis roll and yaw rates, and the expressions for f_i, $i = 1, \ldots, 8$ are given in [36].

Full-Scale Stage 2 Dynamics

The stage 2 dynamics can be written as

$$\begin{bmatrix} \dot{p}_s \\ \dot{q} \\ \dot{r}_s \end{bmatrix} = \begin{bmatrix} f_9(\mathbf{x}) \\ f_{10}(\mathbf{x}) \\ f_{11}(\mathbf{x}) \end{bmatrix} + \begin{bmatrix} \bar{L}_{\delta_a} & 0 & \bar{L}_{\delta_r} \\ 0 & M_{\delta_e} & 0 \\ \bar{N}_{\delta_a} & 0 & \bar{N}_{\delta_r} \end{bmatrix} \begin{bmatrix} \delta_a \\ \delta_e \\ \delta_r \end{bmatrix} \tag{55}$$

where the expressions for f_9, f_{10}, and f_{11} are also given in [36].

To simplify the full-scale equations of the two stages, we introduce the following reasonable assumptions:

1) Sideslip angle β is small; hence $\sin(\beta) \cong 0$, $\cos(\beta) \cong 1$, and $\tan(\beta) \cong 0$.

2) I_{xz} is negligible.

3) Directional acceleration change due to thrust vectoring is negligible.

4) Some forces due to aerodynamic surface deflections are negligible, and so are the lateral force due to α and longitudinal forces due to β.

5) The rate of change of velocity is negligible.

6) Yawing moment due to aileron deflection, rolling moment due to rudder deflection, and $\bar{L}_{\delta r}$, $\bar{L}_r$, $\bar{N}_{\delta a}$, and $\bar{N}_p$ are negligible.

These simplifications are regarded as a part of the modeling error in the inversion process.

Simplified Stage 1 Dynamics

For purposes of inverting the design subject to a set of assumptions above, we can eliminate the states associated with the internal dynamics, and reduce Eq. (54) to the following:

$$\begin{aligned} \begin{bmatrix} \dot{p}_s \\ \ddot{\alpha} \\ \ddot{\beta} \end{bmatrix} &= \begin{bmatrix} 0 \\ \hat{f}_2(\mathbf{x},\boldsymbol{\delta}) \\ \hat{f}_4(\mathbf{x},\boldsymbol{\delta}) \end{bmatrix} + \begin{bmatrix} 1 & 0 & 0 \\ -\tan(\beta) & 1 & 0 \\ 0 & 0 & -1 \end{bmatrix} \begin{bmatrix} \dot{p}_s \\ \dot{q} \\ \dot{r}_s \end{bmatrix} \\ &= F(\mathbf{x},\boldsymbol{\delta}) + G(\mathbf{x}) \cdot \mathbf{u}_1 \end{aligned} \tag{56}$$

Simplified Stage 2 Dynamics

Similarly, the stage 2 dynamics can be expressed as

$$\begin{bmatrix} \dot{p}_s \\ \dot{q} \\ \dot{r}_s \end{bmatrix} = \begin{bmatrix} \hat{f}_9(\mathbf{x}) \\ \hat{f}_{10}(\mathbf{x}) \\ \hat{f}_{11}(\mathbf{x}) \end{bmatrix} + \begin{bmatrix} \bar{L}_{\delta_a} & 0 & 0 \\ 0 & M_{\delta_e} & 0 \\ 0 & 0 & \bar{N}_{\delta_r} \end{bmatrix} \begin{bmatrix} \delta_{ac} \\ \delta_{ec} \\ \delta_{rc} \end{bmatrix} \tag{57}$$

where $\bar{L}_{\delta_a}$, M_{δ_e}, and $\bar{N}_{\delta_r}$ are control effectiveness functions. It is noted that nonlinear functions, $\hat{f}_i(\mathbf{x},\boldsymbol{\delta})$, $i = 2, 4$ in Eq. (56) and $\hat{f}_j(\mathbf{x})$, $j = 9$, 10, and 11 in Eq. (57) are much simpler than those in full-scale dynamics.

2. *Control Allocation with Thrust Vector Control and Differential Tail*

Consider the stage 2 dynamic equation (57) expressed as

$$\dot{\mathbf{x}}_2 = A(\mathbf{x}) + B(\mathbf{x})\mathbf{u}_2 \qquad \mathbf{y}_2 = \mathbf{x}_2 \tag{58}$$

where

$$A(\mathbf{x}) = [\, \hat{f}_9(\mathbf{x}) \quad \hat{f}_{10}(\mathbf{x}) \quad \hat{f}_{11}(\mathbf{x})\,]^T \tag{59}$$

$$B(\mathbf{x}) = \begin{bmatrix} \bar{L}_{\delta a} & 0 & L_{\mathrm{DT}} & 0 & L_{\mathrm{TV}} & 0 & L_{\mathrm{TV}} & 0 \\ 0 & M_{\delta e} & 0 & 0 & M_{\mathrm{DT}} & 0 & M_{\mathrm{TV}} & 0 \\ 0 & 0 & N_{\mathrm{DT}} & \bar{N}_{\delta r} & 0 & N_{\mathrm{TV}} & 0 & N_{\mathrm{TV}} \end{bmatrix} \tag{60}$$

$$\mathbf{x}_2 = [\, p_s \quad q \quad r_s\,]^T \tag{61}$$

$$\mathbf{u}_2 = [\, \delta_a \quad \delta_e \quad \delta_{\mathrm{DT}} \quad \delta_r \quad \delta_{p1} \quad \delta_{y1} \quad \delta_{p2} \quad \delta_{y2}\,]^T \tag{62}$$

δ_a is an aileron deflection, δ_e is an elevator deflection, δ_{DT} is the differential stabilator/tail, δ_r is a rudder deflection, δ_{p1}, δ_{y1} are the pitch and yaw vectoring angles of the left engine, and δ_{p2}, δ_{y2} are the pitch and yaw vectoring angles of the right engine.

A control allocation matrix is introduced to map the effective control demand associated with each axis to the actual controls. Letting $\mathbf{u}_e = [\, \delta_{ac} \quad \delta_{ec} \quad \delta_{rc}\,]^T$ denote the effective control demand, then

$$\mathbf{u}_2 = T_a \cdot \mathbf{u}_e \tag{63}$$

where

$$T_a = \begin{bmatrix} 1 & 0 & 0.5 & 0 & S_p & 0 & -S_p & 0 \\ 0 & 1 & 0 & 0 & S_\alpha & 0 & S_\alpha & 0 \\ 0 & 0 & 0 & 1 & 0 & S_\beta & 0 & S_\beta \end{bmatrix}^T \tag{64}$$

From Eqs. (63) and (64), it can be seen that the roll component of $\mathbf{u}_e$ is allocated to the aileron, differential stabilator, and differential pitch thrust vector deflections, the pitch component of $\mathbf{u}_e$ is allocated to symmetric tail (elevator) and symmetric pitch thrust vector deflections, and the yaw component of $\mathbf{u}_e$ is allocated to rudder and symmetric yaw thrust vector deflections. Therefore, control redundancy exists in all three channels.

3. *Thrust Vector Scheduling*

Thrust vector scheduling variables S_p, S_α, and S_β in Eq. (64) depend on the ratio of the peak moments available from aerodynamic and thrust vector control. For roll channel, the variable S_p is, for instance, defined according to

$$S_p = \begin{cases} 0, & L_{\mathrm{TV}} < \frac{1}{2} L_{\mathrm{aero}} \\ 2 - \frac{L_{\mathrm{aero}}}{L_{\mathrm{TV}}}, & \frac{1}{2} L_{\mathrm{aero}} \le L_{\mathrm{TV}} \le L_{\mathrm{aero}} \\ 1, & L_{\mathrm{TV}} > L_{\mathrm{aero}} \end{cases} \tag{65}$$

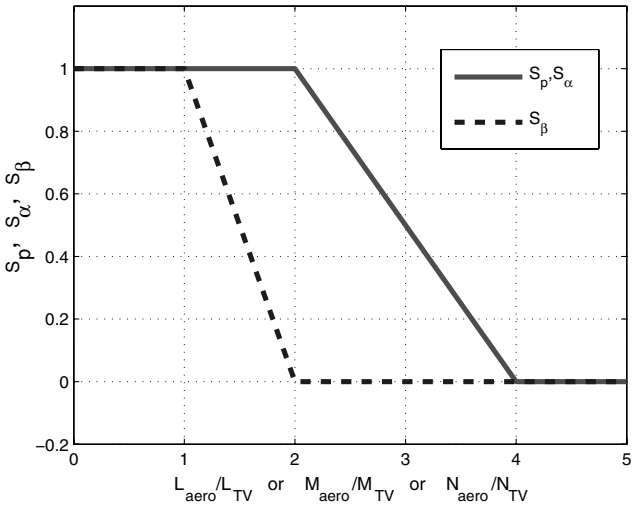

Fig. 6 Shape of thrust-vector scheduling variables.

where L_{aero} is the rolling moment margin available from aerodynamic controls and L_{TV} is the marginal rolling moment available from thrust vector controls [46]. The variables S_α and S_β are defined by similar formulas [10,36]. Thrust vector scheduling is depicted in Fig. 6.

4. Computation of Effective Control ($\mathbf{u}_e$)

From Eq. (58) it follows that

$$\dot{\mathbf{y}}_2 = \dot{\mathbf{x}}_2 = A(\mathbf{x}) + B(\mathbf{x})\mathbf{u}_2 = A(\mathbf{x}) + B(\mathbf{x}) \cdot T_a \mathbf{u}_e = \mathbf{u}_1 \quad (66)$$

The stage 1 dynamic equation is given as

$$\dot{\mathbf{y}}_1 = F(\mathbf{x}) + G(\mathbf{x})\mathbf{u}_1 = \boldsymbol{\nu} \quad (67)$$

where $\boldsymbol{\nu}$ is the pseudocontrol. Combining Eqs. (66) and (67), we have

$$\mathbf{u}_e = (\hat{G}(\mathbf{x})\hat{B}(\mathbf{x})T_a)^{-1}[\boldsymbol{\nu} - (\hat{F}(\mathbf{x}) + \hat{G}(\mathbf{x})\hat{A}(\mathbf{x}))] \quad (68)$$

where $\hat{G}(\mathbf{x})$, $\hat{B}(\mathbf{x})$, $\hat{F}(\mathbf{x})$, and $\hat{A}(\mathbf{x})$ denote estimates of $G(\mathbf{x})$, $B(\mathbf{x})$, $F(\mathbf{x})$, and $A(\mathbf{x})$. Substitution of Eq. (68) into Eq. (63) provides the commanded control that is applied to the aircraft.

5. Pseudocontrol Hedging

PCH is used to address NN adaptation difficulties arising from various actuation nonlinearities, including actuator position and/or rate saturation, discrete (magnitude quantized) control, time delays, and actuator dynamics [34]. NN training difficulties occur when unmodeled or noninvertible actuator characteristics are encountered, as the NN adaptive element will attempt to adapt to them, even when it is impossible to do so. The goal of PCH is to prevent the adaptive element from adapting to these characteristics, while not affecting NN adaptation to other sources of inversion error. Conceptually, PCH "moves the reference model backwards" by an estimate of the amount the controlled system did not move due to selected actuator characteristics (such a position and rate limits, time delays, etc.). The reference model is hedged according to an estimate of the difference between the commanded and achieved pseudocontrol.

The hedge signal is defined as

$$\boldsymbol{\nu}_h = \boldsymbol{\nu} - \hat{\boldsymbol{\nu}} \quad (69)$$

where $\boldsymbol{\nu}$ is the commanded pseudocontrol as defined in Eq. (67), and $\hat{\boldsymbol{\nu}}$ is an estimate for the achieved pseudocontrol. The estimate is obtained by combining Eqs. (63), (66), and (67) and replacing the elements of $\mathbf{u}_2$ by estimates obtained from discrete actuator models of the form in Fig. 7a. Thus,

$$\boldsymbol{\nu}_h = \boldsymbol{\nu} - [\hat{F}(\mathbf{x}) + \hat{G}(\mathbf{x})\hat{A}(\mathbf{x}) + \hat{G}(\mathbf{x})\hat{B}(\mathbf{x}) \cdot \hat{\mathbf{u}}_2] \quad (70)$$

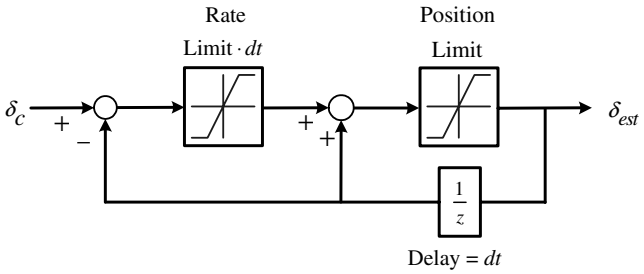

a) Actuator estimator

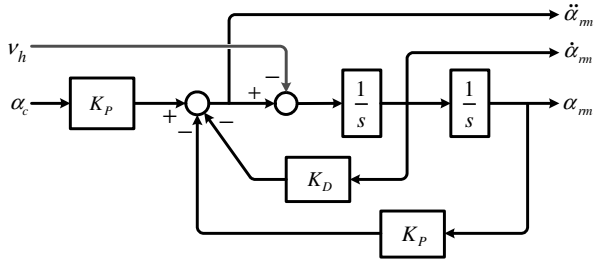

b) Reference model with hedging signal

Fig. 7 Actuator estimator and reference model in pitch channel for PCH.

The elements of the hedge signal are then subtracted in the reference models for each respective axis (roll, pitch, and yaw). The manner in which this is done for a second-order reference model is depicted in Fig. 7b.

VI. Simulation Results

A. Control Design Parameters

With reference to Eqs. (27) and (30), a dynamic compensator for the second ordered α and β channels which have relative degree 2 as shown in Fig. 8 is designed as

$$\boldsymbol{\nu}_{\text{dc}} = K_e \cdot \mathbf{E} = [\,K_P \quad K_D\,] \cdot \mathbf{E} \quad (71)$$

and the tracking error dynamics are given by

$$\dot{\mathbf{E}} = A_M \mathbf{E} + B(\boldsymbol{\nu} - \Delta) \qquad A_M = \begin{bmatrix} 0 & 1 \\ -K_P & -K_D \end{bmatrix} \qquad B_e = \begin{bmatrix} 0 \\ 1 \end{bmatrix} \quad (72)$$

The gains are related to the natural frequency and damping ratio by

$$K_P = \omega_n^2, \qquad K_D = 2\zeta\omega_n \quad (73)$$

Since $r = 1$ in the roll channel, a first-order reference model is employed for that channel, with a time constant of 0.3 s. Likewise, second-order reference models are employed in the pitch and directional channels, with $\omega_n = 3$ rad/s and $\zeta = 1.5$. The values selected are given in Table 1.

Following the approach suggested in Appendix B of [34], we choose

$$Q = \begin{bmatrix} \zeta\omega_n^5 & 0 \\ 0 & \zeta\omega_n^3 \end{bmatrix} = \begin{bmatrix} 364.3 & 0 \\ 0 & 40.5 \end{bmatrix} \quad (74)$$

Table 1 F-15 ACTIVE neural network parameters

Channel	Γ_v	Γ_w	κ_v, κ_w	n_1	n_2	d, s
p_s	3.0	3.0	0.5	23	10	0.01
α	5.0	4.0	0.1	23	10	0.01
β	3.0	3.0	0.1	23	10	0.01

Table 2 F-15 ACTIVE control effectors and their dynamic constraints

Name	Symbol	Magnitude limits, deg	Rate limits, deg/s	Remark
Aileron	δ_a	$-20-+20$	± 100	——
Stabilator	δ_e	$-25-+25$	± 46	——
Differential Stabilator	δ_{DT}	$-25-+25$	± 46	$\delta_{\mathrm{DT}} = (\delta_{e_{\mathrm{right}}} - \delta_{e_{\mathrm{left}}})/2$
Rudder	δ_r	$-30-+30$	± 105	——
TVC nozzle	δ_p, δ_y	20 in any direction	± 80	$\left(\delta_p^2 + \delta_y^2\right)^{1/2} \leq 20$

The activation potentials (a_i) were uniformly distributed between 0.1 and 0.5. In addition, the first NN basis function was used to provide a bias term ($a_0 = 0$). The actuator limits are given in Table 2.

The unsteady aerodynamic effect described earlier was implemented in the pitch axis. This effect has little impact on the lateral modes. The unstable lateral/directional aerodynamic damping coefficients have a significant impact on the responses of the aircraft during high-α maneuvers.

B. Control Design and Simulation Results

The 6-DOF (degree of freedom) F-15 aircraft dynamic model is obtained from [47]. The model has a complete set of lookup tables of aerodynamic coefficients as functions of Mach, α, β, altitude, and aerodynamic control deflections, which is populated up to $\alpha = 60$ deg. This simulation was modified to include TVC (used in the F-15 ACTIVE [38]), differential tail control and RSS as described in Sec. V. A more complete description of the model is given in [36].

All simulations begin from a trimmed flight condition at Mach 0.32 at an altitude of 5000 m. The thrust magnitude is held constant. The controller is implemented in discrete form using a sample rate of 100 Hz. PCH is used only when adaptation is employed. Sensor dynamics and sensor errors are not simulated.

1. *High-α Maneuver*

Simulation results are presented in Figs. 9–13 for a 40-deg α command combined with a 5 deg/s doublet in p_s. Figure 9 shows the α responses for various conditions: with and without RSS, TVC, and adaptation (NN/PCH). Figure 10 shows the p_s and β responses with/without adaptation. At time 0, α begins from its trim value of 11.5 deg and initially follows the reference commanded value of 0 deg. Subsequently at 5 s, a command of 40 deg is applied. The large α command results in position and rate saturation of the actuators, which lead to a response with about 5 deg overshoot in α response. For the system with adaptation, excellent tracking is achieved by about 7–8 s, even though the actuators have periods of rate saturation. The hedged reference command in Fig. 9 cannot be distinguished from the response at this scale.

With no adaptation, the aircraft exhibits a slightly oscillatory error at high α, and has difficulty returning to $\alpha = 0$. The transient response without adaptation during the 40-deg α time interval seems not much different from that with adaptation. The removal of the steady-state error could probably be achieved by adding integral action to the baseline inverting controller, but that would make it considerably more vulnerable to a modeling error as well. The most important improvement derived from NN adaptation is apparent in the lateral/directional channels as shown in Fig. 10. It can be also seen in Fig. 9 that α without adaptation does not follow the command when the commanded α is zero. This is due to the approximations described in Sec. , and thus its performance is limited even at low α. The objective in designing the baseline controller was to achieve the best possible tracking performance at high α, and minimal emphasis was placed on tracking performance at low α. No attempt was made to improve the baseline tracking performance at low α. With adaptation, tracking performance at both low and high α is improved.

The response without RSS shows the motivation for relaxing static stability, namely, that the aircraft does not have enough control authority to reach high α without this relaxation. It is also interesting to note that, without TVC, the aircraft does not return from 40 to 0 deg due to lack of control power without TVC, but does so nicely with TVC. This is the most important contribution that TVC makes to

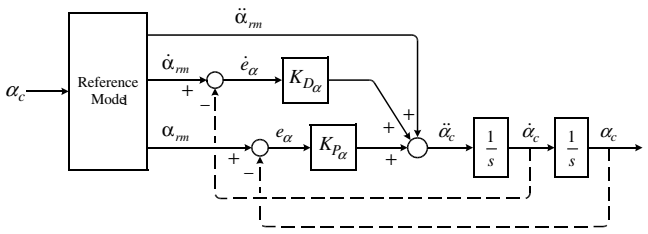

Fig. 8 Structure of a second-order relative degree pitch channel linear controller.

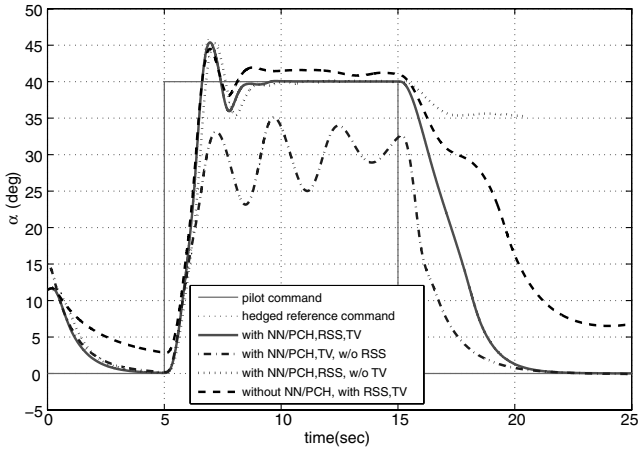

Fig. 9 Aircraft α responses for a high-α command with/without NN adaptation.

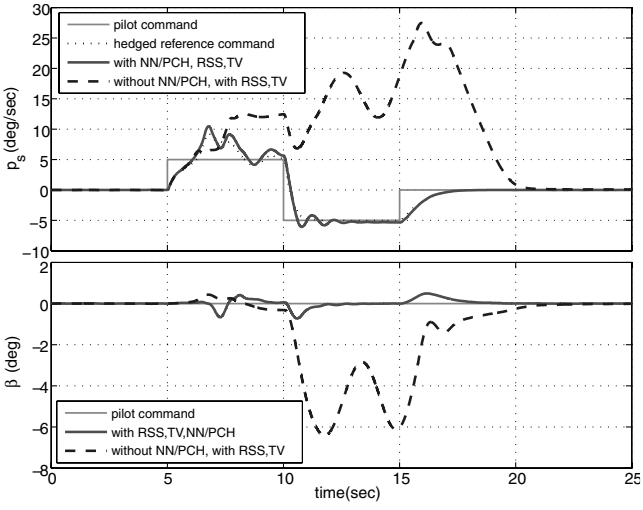

Fig. 10 Aircraft P_s and β responses for a high-α command with/without NN adaptation.

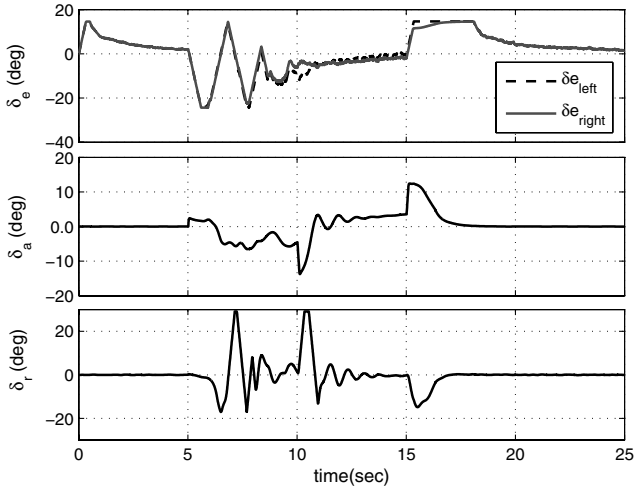

a) With NN/PCH adaptation

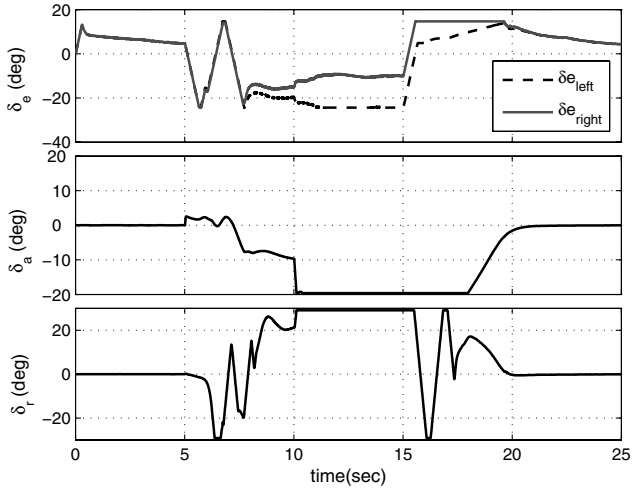

b) Without NN/PCH adaptation

Fig. 11 Aerodynamic control deflections for a high-α command with/without NN adaptation.

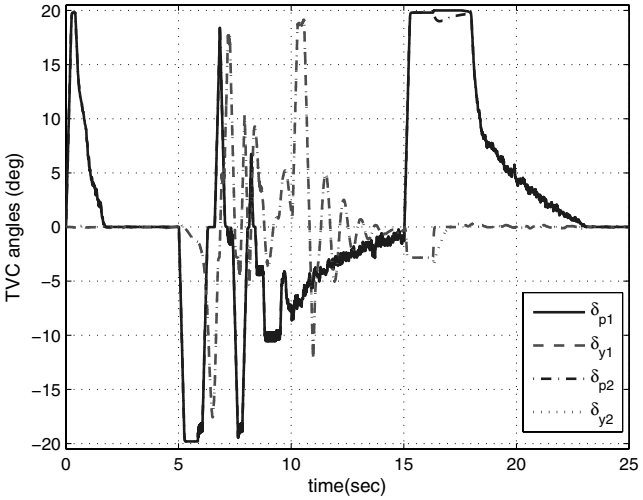

a) With NN/PCH adaptation

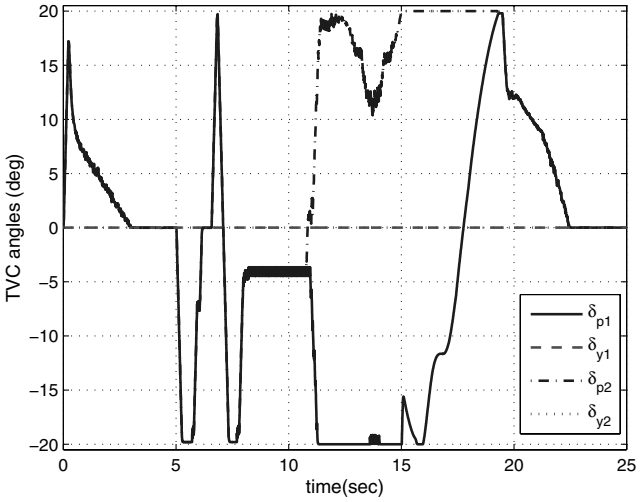

b) Without NN/PCH adaptation

Fig. 12 Thrust vector controls for a high-α command with/without NN adaptation.

the response. Also, the lateral/directional responses are terrible without TVC (not shown).

The p_s response in Fig. 10 exhibits an oscillatory divergence without adaptation, whereas with adaptation the response is stable and accurately follows the hedged reference command in both p_s and β responses. Figure 10 shows that there are large errors in β when no adaptation is present. The oscillation and hedging that appears in the roll channel around 6–10 s is due to the rate and position limiting that is occurring in the TVC pitch control. This can be seen from Fig. 12 which shows that the differential TVC is zero. It can be seen from Figs. 11 and 12 that the small oscillations in sideslip are due to rate and position limiting in rudder and TVC yaw control. In general, all of the oscillations that appear in Figs. 9 and 10 are due to actuator limiting in one form or another. The role that hedging plays in maintaining a stable response is very apparent from these figures.

Time histories of aerodynamic and thrust vector controls for cases with and without adaptation are depicted in Figs. 11 and 12. Note that lateral deflections are not commanded in the case without adaptation, whereas they play a significant role in the case with adaptation. Figure 11 shows that, without adaptation, differential elevator deflection is used when the aileron is saturated. However at high α flight, aerodynamic control is ineffective. Without adaptation, controls are defined through Eqs. (64) and (65) without any provision made for dealing with control saturation. This is not a problem with dynamic inversion itself but a problem in developing a suitable approach to handling control saturation in the nonadaptive case. An advantage of PCH is that one need not worry about what should be done if saturation occurs. It is handled via this approach without the need for introducing additional control allocation logic. Note in Fig. 12a that with adaptation the pairs δ_{p1}, δ_{p2} and δ_{y1}, δ_{y2} are equal except for small differences in the time interval between 16 and 18 s.

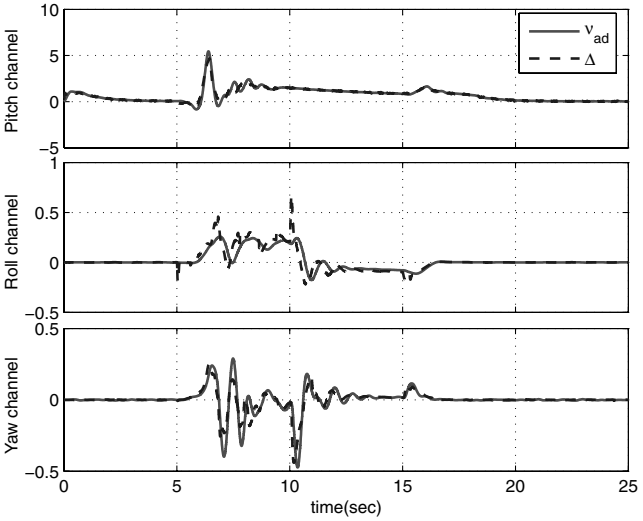

Fig. 13 NN adaptation signal $\nu_{ad}(t)$ and $\Delta(t)$ in pitch, roll, and yaw channels.

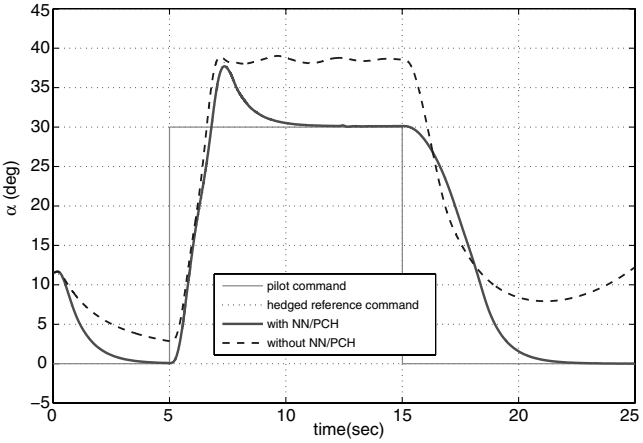

Fig. 14 Aircraft α responses for α/p_s command with/without NN adaptation.

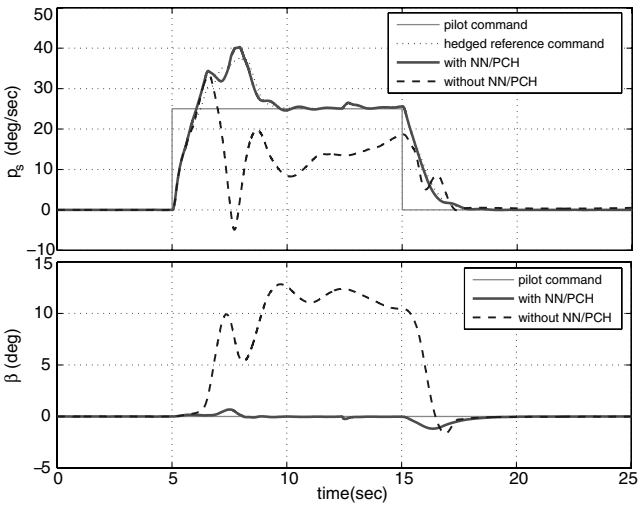

Fig. 15 Aircraft P_s and β responses for α/p_s command with/without NN adaptation.

Whereas, in the case without adaptation, Fig. 12b shows a large demand for differential thrust vectoring ($|\delta_{p1} - \delta_{p2}|$) in the pitch plane due to saturation, and both δ_{y1} and δ_{y2} are zero.

The NN adaptation signal $\boldsymbol{\nu}_{\text{ad}}(t)$ and inversion error $\boldsymbol{\Delta}(t)$ for all channels are compared in Fig. 13. This represents a measure of the degree that adaptation is able to compensate for inversion error. Note that during periods of control saturation, $\boldsymbol{\nu}_{\text{ad}}(t)$ accurately tracks $\boldsymbol{\Delta}(t)$ even though the control is saturated (adaptation while not in control). Thus adaptive control smoothly resumes once the actuation comes out of saturation.

2. *Simultaneous α and p_s Maneuvers*

Simulation results for simultaneous commands of $\alpha = 30$ deg and $p_s = 25$ deg/s are depicted in Figs. 14–18. Figure 14 shows the aircraft angle-of-attack responses for cases with and without adaptation, and Fig. 15 depicts p_s and β responses. It can be seen that with adaptation, good tracking is maintained, except for the oscillation in roll response. As with the previous simulation, unstable lateral/directional aerodynamic characteristics at high α induce the overshoot in the roll axis. Without adaptation, there are large tracking errors, with nearly 10-deg steady-state error in α, a large error in β response, and there is a total lack of command following in the p_s channel. Actuator limiting is most apparent in the time period between 6 and 8 s. The results shown in Fig. 17 are analogous to that observed in Fig. 12. Figure 18 compares $\boldsymbol{\nu}_{\text{ad}}(t)$ and $\boldsymbol{\Delta}(t)$ for all three channels. In all cases, $\boldsymbol{\nu}_{\text{ad}}(t)$ accurately tracks $\boldsymbol{\Delta}(t)$ indicating that saturation is the ultimate limiting factor.

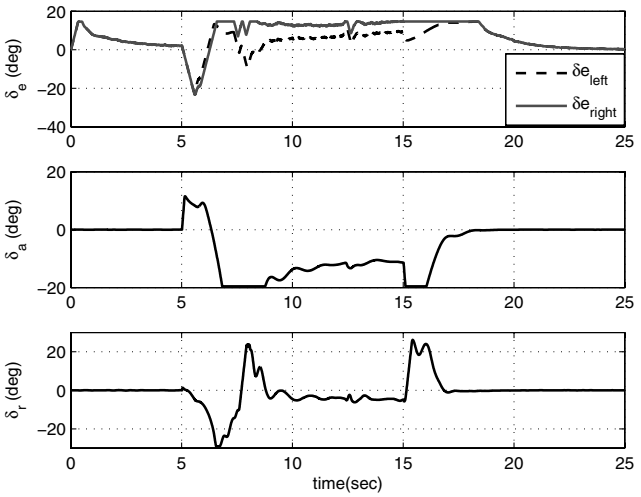

a) With NN/PCH adaptation

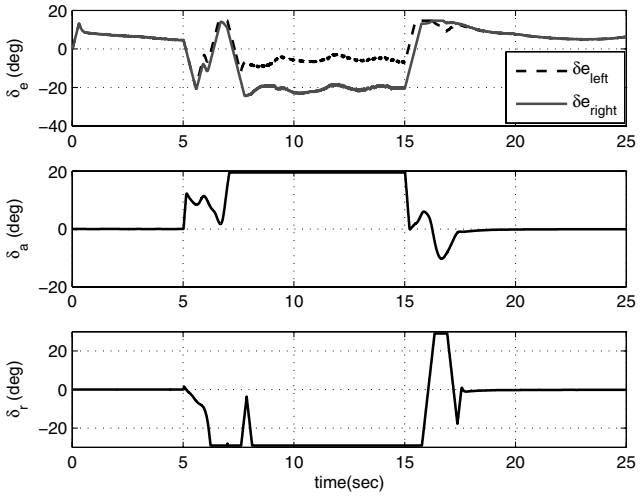

b) Without NN/PCH adaptation

Fig. 16 Aerodynamic control deflections for α/p_s command with/without NN adaptation.

3. *Additional Remarks on Numerical Comparisons*

In comparing the with and without adaptation responses in Figs. 9–17, and particularly the control responses in Figs. 11, 12, 16, and 17, one can easily reach the conclusion that the inverting controller design is flawed. The reader should keep in mind that these cases were chosen to expose the weaknesses in that design. In particular, unsteady aerodynamic effects and unstable damping at high α are not accounted for in the inverting design. These effects lead to control saturation, which is a dominant feature of these results. Whenever the baseline controller becomes unstable it typically enters saturation and remains there. However, the adaptive controller, if it goes into saturation, leaves it gracefully because the adaptive part of the control design is always nearly canceling $\boldsymbol{\Delta}$, even when the control is saturated (adaptation when not in control). This is a key feature in adaptive control that would not be present in a nonadaptive system even if some means were provided for avoiding control saturation. In other words, in adaptive control with PCH the strategy is not to avoid saturation, but to exit saturation in a graceful manner.

VII. Conclusions

This paper evaluates a dynamic inversion-based output feedback adaptive control design for aircraft operating in highly nonlinear flight regimes. A new approach to the treatment of the error dynamics is employed. The approach avoids the introduction of dynamic compensation and is considerably simpler to analyze and implement.

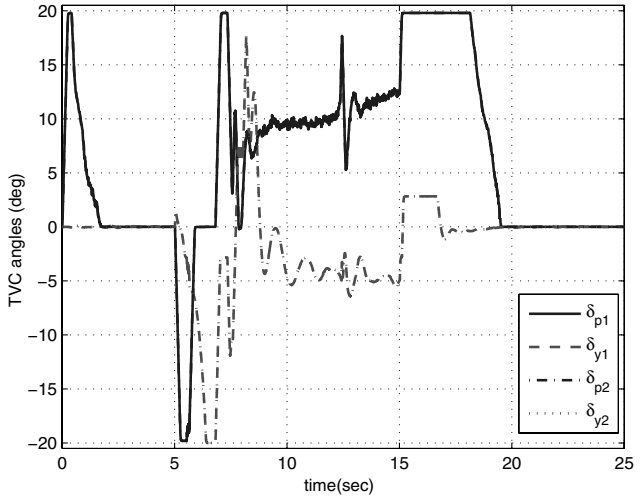

a) With NN/PCH adaptation

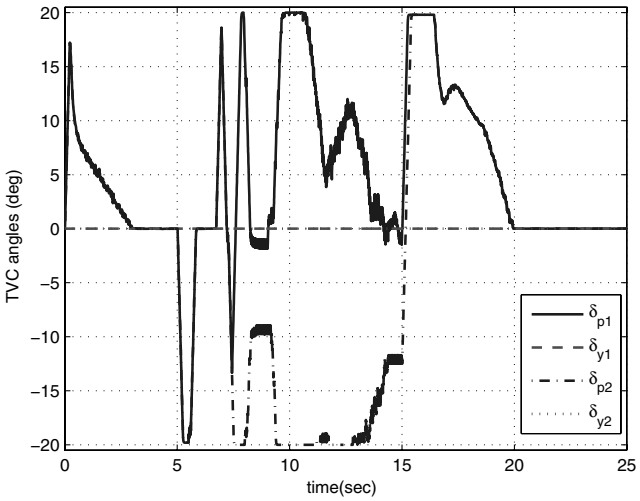

b) Without NN/PCH adaptation

Fig. 17 Thrust vector controls for α/p_s command with/without NN adaptation.

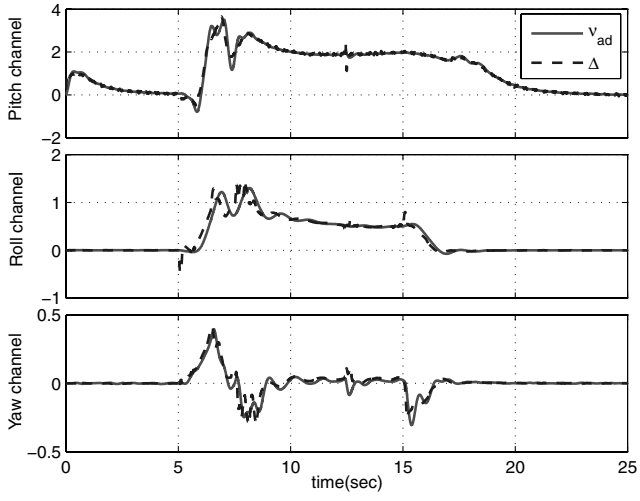

Fig. 18 NN adaptation signal $\nu_{\text{ad}}(t)$ and $\Delta(t)$ in pitch, roll, and yaw channels for α/p_s command.

Stability analysis of the adaptive control system using Lyapunov theorems provides conditions under which the error signals and internal signals are guaranteed to be uniformly ultimately bounded. The stability analysis is considerably streamlined by employing a matching condition assumption.

The resulting adaptive controller was implemented and demonstrated using a 6-DOF nonlinear model based on the NASA F-15 ACTIVE aircraft. Pseudocontrol hedging was found to be particularly important in high angle-of-attack flight because actuator position and rate limits are commonly encountered in this regime. Also critical is the allocation applied to various control effectors and the manner in which adaptive control is implemented to take this allocation into account.

Appendix: Proof of Theorem 1, Adaptive Nonlinear Dynamic Inversion Control Using SHL Neural Networks

Proof. Consider the following Lyapunov function candidate:

$$\mathcal{L}(\mathbf{E},\tilde{\mathbf{E}},\tilde{V},\tilde{W}) = \mathbf{E}^T P\mathbf{E} + \tilde{\mathbf{E}}^T\tilde{P}\,\tilde{\mathbf{E}} + \text{tr}\left(\tilde{W}^T\Gamma_w^{-1}\tilde{W}\right) + \text{tr}\left(\tilde{V}^T\Gamma_v^{-1}\tilde{V}\right) \tag{A1}$$

The time derivative of V along the trajectories of Eqs. (31) and (35) implies

$$\begin{aligned}\dot{\mathcal{L}} &= 2\mathbf{E}^T P\dot{\mathbf{E}} + 2\tilde{\mathbf{E}}^T\tilde{P}\,\dot{\tilde{\mathbf{E}}} - 2\,\text{tr}\left(\tilde{W}^T\Gamma_w^{-1}\dot{\hat{W}}\right) - 2\,\text{tr}\left(\tilde{V}^T\Gamma_v^{-1}\dot{\hat{V}}\right)\\ &= 2\mathbf{E}^T PA_M\mathbf{E} - 2\mathbf{E}^T PB(\boldsymbol{\Delta} - \boldsymbol{\nu}_{\text{ad}} + \mathbf{d} - K_e\tilde{\mathbf{E}})\\ &\quad + 2\tilde{\mathbf{E}}^T\tilde{P}\,\tilde{A}\,\tilde{\mathbf{E}} - 2\tilde{\mathbf{E}}^T\tilde{P}B(\boldsymbol{\Delta} - \boldsymbol{\nu}_{\text{ad}} + \mathbf{d} - K_e\tilde{\mathbf{E}})\\ &\quad - 2\text{tr}\left(\tilde{W}^T\Gamma_w^{-1}\dot{\hat{W}}\right) - 2\text{tr}\left(\tilde{V}^T\Gamma_v^{-1}\dot{\hat{V}}\right)\end{aligned} \tag{A2}$$

Substituting the σ-modification laws in Eq. (13) while recalling $\tilde{\mathbf{E}} = \mathbf{E} - \hat{\mathbf{E}}$, and the relation in Eq. (15), Eq. (A2) becomes

$$\begin{aligned}\dot{\mathcal{L}} &= 2\mathbf{E}^T PA_M\mathbf{E} + 2\tilde{\mathbf{E}}^T\tilde{P}\,\tilde{A}\,\tilde{\mathbf{E}} - 2\tilde{\mathbf{E}}(PB + \tilde{P}B)(\tilde{W}^T(\hat{\boldsymbol{\sigma}} - \hat{\boldsymbol{\sigma}}'\hat{V}^T\boldsymbol{\mu})\\ &\quad + \hat{W}^T\hat{\boldsymbol{\sigma}}'\tilde{V}^T\boldsymbol{\mu}) - 2(\mathbf{E}PB + \tilde{\mathbf{E}}\,\tilde{P}\,B)(\boldsymbol{\varepsilon} - \mathbf{w} + \mathbf{d})\\ &\quad + 2(\mathbf{E}PB + \tilde{\mathbf{E}}\,\tilde{P}\,B)K_e\tilde{\mathbf{E}} + 2\kappa_w\cdot\text{tr}(\tilde{W}^T(\hat{W} - W_0))\\ &\quad + 2\kappa_v\cdot\text{tr}(\tilde{V}^T(\hat{V} - V_0))\end{aligned} \tag{A3}$$

Considering Eqs. (32) and (36) yields

$$\begin{aligned}\dot{\mathcal{L}} &\le -\lambda_{\min}(Q)\|\mathbf{E}\|^2 - \lambda_{\min}(\tilde{Q})\|\tilde{\mathbf{E}}\|^2 - 2\tilde{\mathbf{E}}(PB + \tilde{P}B)(\Delta - \boldsymbol{\nu}_{\text{ad}})\\ &\quad + 2(\tilde{\mathbf{E}} - \mathbf{E})PB(\boldsymbol{\varepsilon} - \mathbf{w} + \mathbf{d}) + 2(\mathbf{E}PB + \tilde{\mathbf{E}}\,\tilde{P}\,B)K_e\tilde{\mathbf{E}}\\ &\quad - \kappa_w\|\tilde{W}\|_F^2 + \kappa_w\|W - W_0\|_F^2 - \kappa_v\|\tilde{V}\|_F^2 + \kappa_v\|V - V_0\|_F^2\end{aligned} \tag{A4}$$

where the following was used:

$$\begin{aligned}\text{tr}(\tilde{W}^T(\hat{W} - W_0)) &\le \|\tilde{W}\|_F\|W - W_0\|_F - \|\tilde{W}\|_F^2\\ &\le -\tfrac{1}{2}\|\tilde{W}\|_F^2 + \tfrac{1}{2}\|W - W_0\|_F^2\end{aligned} \tag{A5}$$

Considering Eqs. (16) and (18) results in

$$\begin{aligned}\dot{\mathcal{L}} &\le -\lambda_{\min}(Q)\|\mathbf{E}\|^2 - \lambda_{\min}(\tilde{Q})\|\tilde{\mathbf{E}}\|^2 + 2\|\tilde{\mathbf{E}}\|(\|PB\|\\ &\quad + \|\tilde{P}B\|)(\alpha_1\|\tilde{Z}\|_F + \alpha_2) + 2(\|\tilde{\mathbf{E}}\| + \|\mathbf{E}\|)\|PB\|(\gamma_1\|\tilde{Z}\|_F\\ &\quad + \gamma_2 + d_m) + 2k_{em}(\|\mathbf{E}\|\,\|PB\| + \|\tilde{\mathbf{E}}\|\,\|\tilde{P}B\|)\|\tilde{\mathbf{E}}\|\\ &\quad - \kappa_w\|\tilde{W}\|_F^2 + \kappa_w\|W - W_0\|_F^2 - \kappa_v\|\tilde{V}\|_F^2 + \kappa_v\|V - V_0\|_F^2\end{aligned} \tag{A6}$$

Assigning $p_a = \max\{\|PB\|, \|\tilde{P}B\|\}$, $\kappa_a = \min\{\kappa_v, \kappa_w\}$, and using completion of squares yields

$$\dot{\mathcal{L}} \le -(\lambda_{\min}(Q) - \gamma_1\|PB\|(1+\gamma_2+d_m) - 2p_a k_{em})\|\mathbf{E}\|^2 - (\lambda_{\min}(\tilde{Q}) - 2p_a(\alpha_1+\alpha_2) - \gamma_1\|PB\|(1+\gamma_2+d_m) - 6p_a k_{em})\|\tilde{\mathbf{E}}\|^2 - (\kappa_a - 2\alpha_1 p_a - 2\gamma_1\|PB\|)\|\tilde{Z}\|_F^2 + 2\alpha_1 p_a + 2\gamma_1(\gamma_2+d_m)\|PB\| + \kappa_w\|W-W_0\|_F^2 + \kappa_v\|V-V_0\|_F^2 \tag{A7}$$

Consequently, recalling

$$\|\tilde{Z}\|_F = \left\|\begin{bmatrix}\tilde{W} & 0\\ 0 & \tilde{V}\end{bmatrix}\right\|_F = \|\tilde{W}\|_F + \|\tilde{V}\|_F$$

the right-hand side of Eq. (A7) is negative outside of the following sets:

$$S_E \triangleq \left\{\mathbf{E}\colon \|\mathbf{E}\| \le \sqrt{\frac{2\alpha_1 p_a + 2\gamma_1(\gamma_2+d_m)\|PB\| + \kappa_w\|W-W_0\|_F^2 + \kappa_v\|V-V_0\|_F^2}{\lambda_{\min}(Q) - \gamma_1\|PB\|(1+\gamma_2+d_m) - 2p_a k_{em}}}\right\}$$

$$S_{\tilde{E}} \triangleq \left\{\tilde{\mathbf{E}}\colon \|\tilde{\mathbf{E}}\| \le \sqrt{\frac{2\alpha_1 p_a + 2\gamma_1(\gamma_2+d_m)\|PB\| + \kappa_w\|W-W_0\|_F^2 + \kappa_v\|V-V_0\|_F^2}{\lambda\min(\tilde{Q}) - 2p_a(\alpha_1+\alpha_2) - \gamma_1\|PB\|(1+\gamma_2+d_m) - 6p_a k_{em}}}\right\} \tag{A8}$$

$$S_{\tilde{Z}} \triangleq \left\{\tilde{Z}\colon \|\tilde{Z}\|_F \le \sqrt{\frac{2\alpha_1 p_a + 2\gamma_1(\gamma_2+d_m)\|PB\| + \kappa_w\|W-W_0\|_F^2 + \kappa_v\|V-V_0\|_F^2}{\kappa_a - 2\alpha_1 p_a - 2\gamma_1\|PB\|}}\right\}$$

Therefore it can be concluded that $\dot{\mathcal{L}}(\boldsymbol{\zeta})$ is negative outside the compact set

$$B_\lambda \triangleq \{\boldsymbol{\zeta} \in B_R \mid \|\boldsymbol{\zeta}\| \le \lambda\} \tag{A9}$$

shown in Fig. 2. It can be seen from Eq. (44) that $B_\lambda \subset B_R$. Let β be the maximum value of the Lyapunov function $\mathcal{L}(\boldsymbol{\zeta})$ on the boundary of B_λ as

$$\beta \triangleq \max_{\|\boldsymbol{\zeta}\|=\lambda} \mathcal{L}(\boldsymbol{\zeta}) \tag{A10}$$

Defining the set

$$\Omega_\beta \triangleq \{\boldsymbol{\zeta} | \mathcal{L}(\boldsymbol{\zeta}) \le \beta\} \tag{A11}$$

the conditions in Eqs. (40), (41), and (44), in Assumption 5 ensures $\Omega_\beta \subset \Omega_\alpha$ and thus ultimate boundedness of $\boldsymbol{\zeta}$ with ultimate bound $\chi_1^{-1}(\chi_2(\lambda))$. Assumption 2 further guarantees that all internal signals are ultimately bounded. □

Acknowledgment

This research was supported by NASA Grant No. NAG-1-01117.

References

[1] Lane, S. H., and Stengel, R. F., "Flight Control Design Using Nonlinear Inverse Dynamics," *Automatica*, Vol. 24, No. 4, 1988, pp. 471–483. doi:10.1016/0005-1098(88)90092-1

[2] Snell, S. A., Enns, D. F., and Garrard, W. L., "Nonlinear Inversion Flight Control for a Supermaneuverable Aircraft," *Journal of Guidance, Control, and Dynamics*, Vol. 15, No. 4, July–Aug. 1992, pp. 976–984.

[3] Reiner, J., Balas, G. J., and Garrard, W. L., "Robust Dynamic Inversion for Control of Highly Maneuverable Aircraft," *Journal of Guidance, Control, and Dynamics*, Vol. 18, No. 1, Jan.–June 1995, pp. 18–24.

[4] Kim, B. S., and Calise, A. J., "Nonlinear Flight Control Using Neural Networks," *Journal of Guidance, Control, and Dynamics*, Vol. 20, No. 1, Jan.–Feb. 1997, pp. 26–33.

[5] Wise, K. A., Brinker, J. S., Calise, A. J., Enns, D. F., Elgersma, M. R., and Voulgaris, P., "Direct Adaptive Reconfigurable Flight Control for a Tailless Advanced Fighter Aircraft," *International Journal of Robust and Nonlinear Control*, Vol. 9, No. 14, 1999, pp. 999–1012. doi:10.1002/(SICI)1099-1239(19991215)9:14<999::AID-RNC449>3.0.CO;2-O

[6] Wang, Q., and Stengel, R. F., "Robust Nonlinear Flight Control of a High-Performance Aircraft," *IEEE Transactions on Control Systems Technology*, Vol. 13, No. 1, 2005, pp. 15–26. doi:10.1109/TCST.2004.833651

[7] Brinker, J. S., and Wise, K. A., "Stability and Flying Qualities Robustness of a Dynamic Inversion Aircraft Control Law," *Journal of Guidance, Control, and Dynamics*, Vol. 19, No. 6, Nov.–Dec. 1996, pp. 1270–1277.

[8] Reiner, J., Balas, G. J., and Garrard, W. L., "Flight Control Design Using Robust Dynamic Inversion and Time-Scale Separation," *Automatica*, Vol. 32, No. 11, 1996, pp. 1493–1504. doi:10.1016/S0005-1098(96)00101-X

[9] Calise, A. J., Lee, S., and Sharma, M., "Development of a Reconfigurable Flight Control Law for Tailless Aircraft," *Journal of Guidance, Control, and Dynamics*, Vol. 24, No. 5, Sept.–Oct. 2001, pp. 896– 902.

[10] Shin, Y., Johnson, M., and Calise, A. J., "Neural Network-Based Adaptive Control for Nonlinear Flight Regimes," AIAA 2003-5717, Aug. 2003.

[11] Shin, Y., Calise, A. J., and Motter, M. A., "Application of Adaptive Autopilot Designs for an Un-Manned Aerial Vehicle," AIAA 2005-6166, Aug. 2005.

[12] Funahashi, K.-I., "On the Approximate Realization of Continuous Mappings by Neural Networks," *Neural Networks*, Vol. 2, Aug. 1989, pp. 183–192. doi:10.1016/0893-6080(89)90003-8

[13] Cybenko, G., "Approximation by Superpositions of a Sigmoidal Function," *Mathematics of Control, Signals, and Systems*, Vol. 2, No. 4, 1989, pp. 303–314. doi:10.1007/BF02551274

[14] Sanner, R. M., and Slotine, J. J., "Gaussian Networks for Direct Adaptive Control," *IEEE Transactions on Neural Networks*, Vol. 3, No. 6, 1992, pp. 837–863. doi:10.1109/72.165588

[15] Sadegh, N., "Nonlinear Identification and Control via Neural Networks," *Control Systems with Inexact Dynamic Models, ASME Winter Annual Meeting*, DSC-Vol. 33, American Society of Mechanical Engineers, Fairfield, NJ, Dec. 1991.

[16] Sadegh, N., "A Perceptron Network for Functional Identification and Control of Nonlinear Systems," *IEEE Transactions on Neural Networks*, Vol. 4, No. 6, Nov. 1993, pp. 982–988. doi:10.1109/72.286893

[17] Hornik, K., "Multilayer Feedforward Networks Are Universal Approximators," *Neural Networks*, Vol. 2, No. 5, 1989, pp. 359–366. doi:10.1016/0893-6080(89)90020-8

[18] Lewis, F. L., "Nonlinear Network Structures for Feedback Control," *Asian Journal of Control*, Vol. 1, No. 4, Dec. 1999, pp. 205–228.

[19] Ge, S. S., Hang, C. C., and Zhang, T., "Adaptive Neural Network Control of Nonlinear Systems by State and Output Feedback," *IEEE Transactions on Systems, Man and Cybernetics. Part B. Cybernetics*, Vol. 29, No. 6, Dec. 1999, pp. 818–828. doi:10.1109/3477.809035

[20] Narendra, K. S., and Mukhopadhyay, S., "Adaptive Control of Nonlinear Multivariable Systems Using Neural Networks," *Neural Networks*, Vol. 7, No. 5, 1994, pp. 737–752. doi:10.1016/0893-6080(94)90096-5

[21] Lewis, F. L., Yesildirek, A., and Liu, K., "Multilayer Neural-Net Robot Controller with Guaranteed Tracking Performance," *IEEE Transactions on Neural Networks*, Vol. 7, No. 2, March 1996, pp. 388–399. doi:10.1109/72.485674

[22] Hovakimyan, N., Calise, A. J., and Kim, N., "Adaptive Output Feedback Control of Uncertain Nonlinear Systems Using Single-Hidden-Layer Neural Networks," *IEEE Transactions on Neural Networks*, Vol. 13, No. 6, Nov. 2002, pp. 1420–1431. doi:10.1109/TNN.2002.804289

[23] Hovakimyan, N., Calise, A. J., and Kim, N., "Adaptive Output Feedback Control of a Class of Multi-Input Multi-Output Systems Using Neural Networks," *International Journal of Control*, Vol. 77, No. 15, 2004, pp. 1318–1329. doi:10.1080/00207170420002971 53

[24] Stengel, R. F., "Toward Intelligent Flight Control," *IEEE Transactions on Systems, Man, and Cybernetics*, Vol. 23, No. 6, 1993, pp. 1699–1717. doi:10.1109/21.257764

[25] Werbos, P. J., "Neural Networks and Flight Control—Overview of Capabilities and Emerging Applications," *AIAA Guidance, Navigation and Control Conference*, AIAA, Washington, D.C., Aug. 1995, pp. 912–919; also AIAA 1995-3272.

[26] Williams-Hayes, P. S., "Selected Flight Test Results for Online Learning Neural Network-Based Flight Control System," AIAA 2004-6283, 20–22 Sept. 2004.

[27] Williams-Hayes, P. S., "Flight Test Implementation of a Second Generation Intelligent Flight Control System," NASA Technical Memorandum, NASA-TM-2005-213669, NASA Dryden Flight Research Center, Nov. 2005.

[28] McFarland, M. B., and Calise, A. J., "Multilayer Neural Networks and Adaptive Nonlinear Control of Agile Anti-Air Missiles," *AIAA Guidance, Navigation and Control Conference*, AIAA, Reston, VA, Aug. 1997, pp. 401–410; also AIAA 1997-3540.

[29] Rysdyk, R. T., and Calise, A. J., "Adaptive Model Inversion Flight Control for Tilt-Rotor Aircraft," *Journal of Guidance, Control, and Dynamics*, Vol. 22, No. 3, 1999, pp. 402–407.

[30] Perhinschi, M. G., Napolitano, M. R., Campa, G., Seanor, B., Gururajan, S., and Yu, G., "Design and Flight Testing of Intelligent Flight Control Laws for the WVU YF-22 Model Aircraft," AIAA 2005-6445, Aug. 2005.

[31] Sharma, M., and Calise, A. J., "Neural-Network Augmentation of Existing Linear Controllers," *Journal of Guidance, Control, and Dynamics*, Vol. 28, No. 1, Sept.–Oct. 2005, pp. 12–19. doi:10.2514/1.4144

[32] Leitner, J., Calise, A. J., and Prasad, J. V. R., "Analysis of Adaptive Neural Networks for Helicopter Flight Controls," *Journal of Guidance, Control, and Dynamics*, Vol. 20, No. 5, Sept.–Oct. 1997, pp. 972– 979.

[33] Corban, J. E., Calise, A. J., and Prasad, J. V. R., "Flight Test of an Adaptive Control System for Unmanned Helicopter Trajectory Following," AIAA Paper 2000-4058, Aug. 2000.

[34] Johnson, E. N., "Limited Authority Adaptive Flight Control," Ph.D. Dissertation, Georgia Institute of Technology, School of Aerospace Engineering, Atlanta, GA, Dec. 2000.

[35] Calise, A. J., Shin, Y., and Johnson, M., "Neural Network-Based Adaptive Control for Nonlinear Flight Regimes," NASA Technical Report (Final Report), NASA Langley Research Center, Hampton, VA, March 2006.

[36] Shin, Y., "Neural Network Based Adaptive Control for Nonlinear Dynamic Regimes," Ph.D. Dissertation, Georgia Institute of Technology, School of Mechanical Engineering, Atlanta, GA, Dec. 2005.

[37] Kim, N., and Calise, A. J., "Several Extensions in Methods for Adaptive Output Feedback Control," *IEEE Transactions on Neural Networks*, Vol. 18, No. 2, March 2007, pp. 482–494. doi:10.1109/TNN.2006.885120

[38] Orme, J. S., Hathaway, R., and Ferguson, M. D., "Initial Flight Test Evaluation of the F-15 ACTIVE Axisymmetric Vectoring Nozzle Performance," NASA Technical Memorandum, NASA-TM-1998-206558, NASA Dryden Flight Research Center, July 1998.

[39] Khalil, H. K., *Nonlinear Systems*, 3rd ed., Prentice–Hall, Upper Saddle River, NJ, 2002.

[40] Lavretsky, E., Hovakimyan, N., and Calise, A., "Upper Bounds for Approximation of Continuous-Time Dynamics Using Delayed Outputs and Feedforward Neural Networks," *IEEE Transactions on Automatic Control*, Vol. 48, No. 9, Sept. 2003, pp. 1606–1610. doi:10.1109/TAC.2003.816987

[41] AGARD, *High Angle-of-Attack Aerodynamics*, AGARD Lecture Series No. 121, NATO, June 1983.

[42] Cobleigh, B. R., "High-Angle-of-Attack Yawing Moment Asymmetry of the X-31 Aircraft from Flight Test," NASA Contractor Report, NASA-CR-186030, NASA Dryden Flight Research Center, Sept. 1994.

[43] Bowers, A. H., Pahle, J. W., Wilson, R. J., Flick, B. C., and Rood, R. L., "An Overview of the NASA F-18 High Alpha Research Vehicle," NASA Technical Memorandum, NASA-TM-4772, NASA Dryden Flight Research Center, Oct. 1996.

[44] Sweetman, B., *F-22 Raptor*, Enthusiast Color Series, Motorbooks International, Osceola, WI, 1998.

[45] Klein, V., and Noderer, K. D., "Modeling of Aircraft Unsteady Aerodynamic Characteristics: Part 1–Postulated Models," NASA TM-109120, NASA Langley Research Center, May 1994.

[46] Lallman, F. J., Davidson, J. B., and Murphy, P. C., "A Method for Integrating Thrust-Vectoring and Actuated Forebody Strakes with Conventional Aerodynamic Controls on a High-Performance Fighter Airplane," NASA TP-208464, NASA Langley Research Center, Sept. 1998.

[47] Brumbaugh, R. W., "Aircraft Model for the AIAA Controls Design Challenge," *Journal of Guidance, Control, and Dynamics*, Vol. 17, No. 4, July–Aug. 1994, pp. 747–752; also NASA CR-186019.